Gradu Amaierako Lana / Trabajo Fin de Grado
Fisikako eta Ingeniaritza Elektronikoko Gradu Bikoitza (Ingeniaritza Elektronikoa) /
Doble Grado en Física y en Ingeniería Electrónica (Ingeniería Electrónica)

Over-modeling Reduction in Vector Fitting Identification for Stability Analysis of Microwave and RF Amplifiers

Egilea/Autor/a:
Sara Fernández Uria

Zuzendaria/Director/a:
Aitziber Anakabe Iturriaga
Juan Mari Collantes Metola

Contents

Chapter 1

Introduction and Objectives

1.1 Introduction

Microwave and RF amplifiers are prone to undesired oscillations of different nature due to multiple parasitic feedback loops [1], [2]. Therefore, it is convenient to predict these instabilities in simulation, during the design process of the mentioned devices.

Several stability analysis methods can be found in the literature for the above-mentioned purpose [3]-[8]; however, since its first application to microwave amplifiers in 2001, pole-zero identification [8] has proved to be a very useful and simple tool for the given problem. Its simplicity provides a quick graphical evaluation of the stability: a system is said to be stable when the totality of its poles lies in the Left-Half Plane (LHP) of the complex plane, *i.e.*, when all the real parts of the poles are strictly negative.

To analyze the poles and zeros of the system, pole-zero identification requires the linear (or linearized) transfer function of the system, preferably defined as the ratio of two polynomials. In the current scenario, the transfer function of the circuit will be fitted from the frequency response, using optimization techniques such as least squares, maximum likelihood estimation, vector fitting etc [9]. How to obtain this frequency response will be later detailed, nevertheless, in this essay we will mainly focus on the fitting technique itself. Indeed, quality and reliability of the stability assessment rely substantially on the fitted transfer function.

The foremost problem encountered is guessing the order of the transfer function, which is *a priori* unknown. If the system is under-modeled, part of the dynamics will be missing. On the other hand, if the system is over-modeled, too many parameters will be added to the model and some misleading conclusions could be drawn regarding the stability; non-physical unstable poles could be added to the model, making designers believe a true instability exists in the circuit. Under-modeling is a problem easily controlled with a correct error criteria; over-modeling, however, can be more complex to avoid and it is essentially the principal issue addressed in this essay.

1.2 Objectives

As stated in the precedent section, over-modeling can be a critical problem for microwave circuit designers when doing a pole-zero stability analysis. Hence, in this project we will aim to develop a new technique and strategy to overcome this troublesome issue, or, to the extent possible, minimize its effects. To that end, we will create an automatic algorithm based on the state-of-the-art automatic Vector Fitting

algorithm for stability analysis [10] and a paper authored by S. Grivet-Talocia and M. Bandinu [11].

Moreover, we will implement it in *Matlab*, where —once the transfer function identified— the corresponding pole-zero diagram will be displayed in order to facilitate the interpretation of the results regarding the stability of the device under test.

As an attempt to improve the state-of-the-art method, we will compare thoroughly the identifications carried out by both automatic algorithms. Thus, we will be able to determine the possible advantages of our contribution regarding over-modeling. Furthermore, bearing in mind the general scenario of this project, we will specifically assess the validity of these benefits for the stability analysis of microwave and RF amplifiers.

Lastly, we will conclude by evaluating the limitations of the developed technique and by proposing ideas for a further work.

Chapter 2

Theoretical Framework

In this chapter we will briefly set the theoretical framework of this project: pole-zero stability analysis of microwave and RF amplifiers and the identification method Vector Fitting.

2.1 Pole-Zero Stability Analysis of Microwave and RF Amplifiers

Pole-zero identification consists in the obtaining and the study of the poles and zeros of a linear (or linearized) system's frequency response. In fact, the information regarding the stability of the system underlies the own nature of the poles [8], [12]:

- Poles with negative real part, *i.e.*, laying in the **Left-Half Plane** (LHP), are **stable** and give rise to signals that decay in time.

- Poles with positive real part, *i.e.*, laying in the **Right-Half Plane** (RHP), are **unstable** and give raise to signals that grow in time.

- Poles with null real part, *i.e.*, laying in the **imaginary axis**, give rise to **purely oscillatory** signals.

Returning to the matter in hand —stability analysis of microwave and RF amplifiers— two main steps have to be carried out in order to perform the pole-zero identification [13].

First of all, a closed-loop frequency response of the circuit linearized about its steady state must be calculated. The cited steady state can be either a DC bias point or a large-signal periodic regime forced by the input drive. Moreover, the closed-loop frequency response is obtained "probing" the circuit and sweeping the frequency along the band of examination, either by a small-signal voltage source inserted in series into a circuit branch or by a small-signal current source branched at a circuit node. The frequency response provided by the current source is the impedance seen by the probe at the connection node, whereas the one obtained with the voltage source is the total admittance presented to the probe[1].

Furthermore, having a linear or linearized system, all closed-loop frequency responses will share the same set of poles. Consequently, the discussed frequency response can be either Single-Input Single-Output

---

[1]Other responses such as trans-impedances, trans-admittances or voltage and current transfers are also valid, as long as they are closed-loop and describe the linearized system.

(SISO) or Multiple-Input Multiple-Output (MIMO), since any node or branch of the circuit will render the same stability information. Nonetheless, some nodes and branches of the circuit might be electrically isolated from part of the circuit's dynamics, which materializes in a pole-zero cancellation [10], [13], [14].

Secondly, the frequency response must be fitted to a transfer function, defined as the ratio of two polynomials. For this purpose, several optimization techniques can be used, such as least squares, maximum likelihood estimation, vector fitting etc. As stated earlier, the order of the transfer function is *a priori* unknown and therein lies the fundamental challenge of the identification [9]. Precisely, both under-modeling and over-modeling need to be avoided in the approximation to prevent misleading or partial conclusions concerning the stability [15].

2.2   Vector Fitting Method

As discussed in the former section, the procured frequency response of the system must be fitted to a transfer function by means of an optimization technique. Vector Fitting (VF) [16]-[18] is a general methodology for the fitting of frequency domain responses with rational function approximations, and since it has proved to be very suitable for stability analysis of microwave circuits [10], it will be the one employed in this work. The technique goes as follows: [16]-[18]

The transfer functions are described using a rational function approximation:

$$H_m(s) \approx \sum_{n=1}^{N} \frac{r_{m,n}}{s - p_n} + D_m \,, \tag{2.1}$$

where H_m is the mth component of a vector of transfer functions, $\{p_n\}_{n=1}^{N}$ the poles of the system, $\{r_{m,n}\}_{n=1}^{N}$ the residues, D_m the direct gain and N the order of the transfer function[2].

The approximation is to be computed starting from a set of frequency samples $\{H_m(j\omega_i)\}_{i=1}^{Ns}$ and an initial estimation of the N poles, $\{q_n\}_{n=1}^{N}$. Hereunder, we multiply (2.1) with an unknown function $\sigma(s)$ and set the following problem:

$$\sigma(s)H_m(s) \approx \sum_{n=1}^{N} \frac{\hat{r}_{m,n}}{s - q_n} + \hat{D}_m \qquad \text{where} \qquad \sigma(s) \approx \sum_{n=1}^{N} \frac{\tilde{r}_{m,n}}{s - q_n} + 1 \,. \tag{2.2}$$

This linear system is solved as a Least Squares problem using the available data $\{H_m(jw_i)\}_{i=1}^{Ns}$, leading to the determination of $\{\hat{r}_{m,n}\}$, $\hat{D}_m$ and $\{\tilde{r}_{m,n}\}$.

We notice from (2.2) that the poles of the best rational approximation of $H_m(s)$ must be equal to the zeros of $\sigma(s)$, $\{z_{m,n}\}$, which can be easily calculated from $\hat{D}_m$ and $\{q_n\}$. Taking those as the new set of poles, a new linear problem is appointed to determine the residues $\{r_{m,n}\}$ and direct gain D_m of the transfer function. Thus, this realization gives way to a rational function approximation of the transfer function, whose fitting error might depend in the initial guess of the set of poles.

Moreover, these steps can be repeated setting the final poles determined on the previous iteration as the initial poles for the next one, improving consequently the approximation of the transfer function.

---

[2]Note that both the residues and the direct gain depend on the transfer function, while the set of poles is common for all of them.

Chapter 3

Automatic Identification with Vector Fitting

In this chapter we will firstly describe the state-of-the-art regarding the use of Vector Fitting (VF) (fitting method presented in Section 2.2) in the context of stability analysis of microwave circuits. Secondly, we will expound our contribution to the aforementioned state-of-the-art.

3.1 State-of-the-Art Automatic Vector Fitting Algorithm for Stability Analysis

VF is an iterative algorithm that takes an initial estimate set of poles and, by means of successive simple VF identifications (see Section 2.2), returns an approximation of the transfer function once a desired accuracy is reached or a certain number of iterations is performed. The selection of the order of the transfer function, *i.e.*, number of poles, can be either manual or automatic.

In case of the manual order selection, once the order has been selected by the user, the poles are usually linearly spread in the bandwidth under study, following the instructions in [16]-[18]. Then, a sequence of the above-mentioned iterations is conducted, resulting in an approximation of the transfer function of the chosen order.

Conversely, when the selection of the order is automatic, a more fine algorithm has to be implemented. That is the case of the stability analysis tool *MM_stab* [10], [19], created by L. Mori in *Matlab* based on VF, which computes the minimum order required to satisfy the fitting goal demanded by the user. This goal is determined by the desired phase tolerance of the user, $\theta_{tolerance}$; that is, the maximal absolute phase error (for all the frequency points) between the identified transfer function and the frequency response. Briefly summarizing the algorithm:

1. The lowest order possible for fitting the transfer function is assumed to be two times the number of resonances in the frequency response; that is to say, $N_{min} = 2r$, where r is the number of resonances. To avoid over-modeling in the event of noisy responses, a minimal distance of 5 data points is imposed between the resonances.

2. The initial poles are selected to be complex conjugate poles with weak attenuation and imaginary parts that cover the entire frequency band under study, as indicated by [16]-[18].

3. A first VF identification is carried out, composed by 15 iterations.

4. If the resulting phase error is below the selected phase tolerance $\theta_{tolerance}$ for all the frequencies under study, the identification is stopped.

5. If the phase tolerance is exceeded, the order is increased by two, $N \to N + 2$, and two complex conjugate poles are added in the center of the frequency band.

6. A new identification is carried out and so on, increasing the order iteratively until the maximum error criteria is attained or until the order reaches its maximum allowed value, $N_{max} = 10r$.

A flow diagram that summarizes the automatic identification algorithm is shown in Figure 3.1.
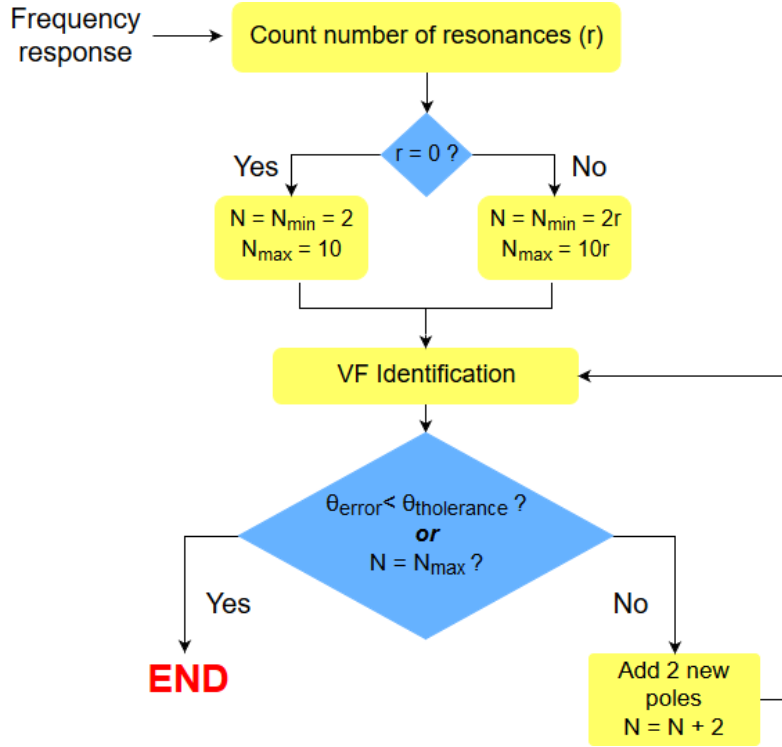

Figure 3.1: Flow diagram of the state-of-the-art automatic VF algorithm for stability analysis.

In addition, to minimize the visualization of mathematical poles caused by over-modeling and improve the interpretation of the results, only resonant poles with magnitude peaks greater than 0.5 dB and resonant frequencies inside the bandwidth are plotted in the pole-zero map. That is to say, only pairs of complex conjugate poles $p = a \pm bj$ meeting these conditions are plotted:

$$\delta = \frac{-a}{\sqrt{a^2 + b^2}} < 0.5785 \qquad \text{and} \qquad w_{min} \leq w_r = \sqrt{b^2 - a^2} \leq w_{max}, \tag{3.1}$$

where δ is the damping factor, w_r the resonant frequency and w_{min} and w_{max} the lower and upper limits of the frequency band under study.

3.2 Proposed Contribution to the State-of-the-Art Automatic Vector Fitting Algorithm for Stability Analysis

Owing to the problematic of over-modeling, a new automatic VF-based identification algorithm has been proposed in this project, grounded on the cited work of L. Mori [10], [19] and a paper authored by S. Grivet-Talocia and M. Bandinu [11]. Certainly, order estimation constitutes the most difficult stage when intending a fully automated identification process and it is expressly what we have attempted to improve.

The main modifications and contributions to the basic VF algorithm introduced in this project are divided in two categories: placing of the added poles and elimination of spurious poles. Additionally, an extra stopping condition has been included in the main iteration loop —along with the phase tolerance and the maximum order— to avoid both convergence issues and over-modeling: a threshold error variation between successive iterations.

$$\delta\theta_{error} < \alpha \langle \theta_{error} \rangle \tag{3.2}$$

Here above $\delta\theta_{error} = |\theta^i_{error} - \theta^{i-1}_{error}|$ and $\langle \theta_{error} \rangle = \frac{1}{2}(\theta^i_{error} + \theta^{i-1}_{error})$ denote the absolute phase error difference between the current and the previous iterations and the average phase error between those two iterations, respectively. The phase error θ_{error} is taken to be the maximum of the absolute phase error.

Likewise, α is a free parameter to delimit the threshold, set by default to 0.001. Indeed, when the error variation between successive iterations reaches this threshold, that is, when equation (3.2) is satisfied, it can be considered that θ_{error} is stalling. Therefore, in order to avoid continuing to increase the order of the transfer function, the identification is stopped.

3.2.1 Placing of the added poles

A modified placing of the added poles has been essentially intended to contribute a valid guess of the placement of the poles before the standard VF pole relocation. It has been implemented both in the determination of the initial set of poles and between the iterations of the standard VF algorithm.

For the determination of the initial set of poles, firstly, just as indicated in Section 3.1, the number of resonances in the frequency response is computed (r) and then, each resonant peak is associated to a pair of complex conjugate poles in the following way:

$$p_{2n-1}{}^{initial} = (-0.01 + j)\,\omega_n\,, \qquad p_{2n}{}^{initial} = (-0.01 - j)\,\omega_n$$
$$\text{for} \quad n \in \{1, ..., r\}\,, \tag{3.3}$$

where $\{w_n\}_{n=1}^r$ are the angular frequencies of the peaks. That is to say, the lowest order possible for fitting the transfer function is established as twice the number of resonances, just as in [10], but instead of spreading the imaginary parts of the poles linearly along the bandwidth, we place each complex conjugate pair in a resonant frequency.

On the other hand, the addition of poles in each iteration is slightly trickier. The basic steps were proposed by the mentioned work of S. Grivet-Talocia and M. Bandinu [11] in the context of convergence improvement for noisy frequency responses, but we have found them to be equally effective to prevent over-modeling. They go as follows:

- We calculate the frequency-dependent error of the actual fitting of each frequency response and its mean value:

$$\Delta(\omega_i) = \max_{1 \leq m \leq M} \left\{ \|H_m^{fit}(j\omega_i) - H_m(j\omega_i)\| \right\}, \tag{3.4}$$

$$\langle \Delta(\omega_i) \rangle = \frac{1}{N_s} \sum_{i=1}^{N_s} \Delta(\omega_i), \tag{3.5}$$

where M is the total number of transfer functions and N_s the total number of frequencies.

Thereupon, we determine the subsequent set of frequencies from our data $\{\omega_i\}_{i=1}^{N_s}$ for which the error is greater than the mean value:

$$\Psi = \{\omega_i : \Delta(\omega_i) > \langle \Delta(\omega_i) \rangle\}. \tag{3.6}$$

- In parallel we define a safety zone around each pole of the actual fitting model where no new poles will be allowed to be placed[1]:

$$\Theta = \bigcup_{n=1}^{N} \Theta_n = \bigcup_{n=1}^{N} \{s : |\text{Re}(s) - \text{Re}(p_n)| < \nu |\text{Re}(p_n)| \\ \text{and} \quad |\text{Im}(s) - \text{Im}(p_n)| < \nu |\text{Im}(p_n)|\}, \tag{3.7}$$

where ν is the minimum distance delimiter, a free parameter of the algorithm set by default to 0.01 after several tests.

- Thereafter, we will construct the set of possible poles to be added:

$$\Pi = \{p = (0.01 \pm j)\,\omega \, : \, \omega \in \Psi \quad \text{and} \quad p \notin \Theta\}. \tag{3.8}$$

Hence, when adding new poles within the algorithm —before VF relocation— we will select them only from this set. For this selection, we will start by choosing those placed in error peaks or regions with higher error and then, if necessary, continue with others placed as far apart as possible.

3.2.2   Elimination of spurious poles

Elimination of spurious poles is probably the most powerful addition to the state-of-the-art VF identification algorithm to counteract our ongoing over-modeling problem. It can be conducted in a variety of ways, but once again, we have employed the method proposed by S. Grivet-Talocia and M. Bandinu [11]:

- For each pair of complex conjugate poles $\{p_n, p_n^*\}$ with residues $\{r_{m,n}, r_{m,n}^*\}$ of the fitted model, we calculate their contribution to the entire transfer function H_m:

$$H_{m,n}(s) = \frac{r_{m,n}}{s - p_n} + \frac{r_{m,n}^*}{s - p_n^*} \quad n \in \{1, ..., N\}. \tag{3.9}$$

- Afterwards, we compute the p-norm for each $H_{m,n}$ over a bandwidth $\Omega_{m,n}$, defined by the -10 dB level of the resonant peak:

$$\mu_{m,n}^{(p)} = \left(\sum_{\omega_i \in \Omega_{m,n}} |H_{m,n}(j\omega_i)|^p \right)^{\frac{1}{p}}, \tag{3.10}$$

where $p \in [1, +\infty)$ is another free parameter of the algorithm, which, as suggested in [11], has been set by default to $p = 2$.

---

[1]It must be clarified that the standard VF relocation could place few poles close to each other; this constraint is only applied to the addition of the poles *before* VF relocation.

- We next calculate the mean value of $\mu_{m,n}^{(p)}$ and the ratio $d_{m,n}$:

$$\langle \mu_{m,n}^{(p)} \rangle = \frac{1}{N} \sum_{n=1}^{N} \mu_{m,n}^{(p)}, \qquad d_{m,n} = \frac{\mu_{m,n}^{(p)}}{\langle \mu_{m,n}^{(p)} \rangle}. \tag{3.11}$$

- Once these values computed, the following poles p_n are considered to be spurious:

$$\max_{1 \leq m \leq M} \{d_{m,n}\} < \gamma \ll 1, \tag{3.12}$$

where M is the total number of transfer functions, in case of a MIMO response, and γ the spurious poles discriminator, parameter of the algorithm set by default to $\gamma = 0.01$.

These poles make a negligible contribution to the total fitting and therefore they will be eliminated. Note that we consider the maximum value of $d_{m,n}$ over all m to avoid the effect of low controllability and/or observability of different nodes.

Having described the kernel of these modifications we will now proceed to explain how to introduce them in the standard VF identification algorithm:

1. We first compute the number of resonances r (with at least 5 data points) and associate a pair of complex conjugate poles with weak attenuation to each peak, as described in Subsection 3.2.1. If no peaks are found, two conjugate poles are placed with their imaginary parts in the middle of the bandwidth under study, as suggested in [16]-[18].

2. We then enter the main iteration loop and initiate the VF identification, composed by N_{iter} iterations, a free parameter to be chosen by the user and set by default to $N_{iter} = 15$.

3. Once these identifications are finished, we will search the number of spurious poles N_{sp} among the recently relocated ones. If no spurious poles are found ($N_{sp} = 0$) we will proceed to check the stopping conditions of the main iteration loop:

$$\theta_{error} < \theta_{tolerance}, \quad N = N_{max} = 10r \quad \text{or} \quad \delta\theta_{error} < \alpha\langle\theta_{error}\rangle.$$

4. On the contrary, if $N_{sp} > 0$ spurious poles are found, we will eliminate those poles and carry out a new VF identification process (fixing the remaining poles) just to obtain the new fitting model. Once these poles have been removed, we verify whether the phase tolerance chosen by the user is respected. If so, the overall identification is terminated and otherwise, N_{sp} new poles from Π are added (see Subsection 3.2.1).

5. Right after, we conduct another VF identification and, once finished, we check the stopping conditions of the main iteration loop.

6. Just as in the standard identification algorithm, if none of these conditions are respected, the order will be increased by two —adding two poles from Π, following the criteria thoroughly explained in Subsection 3.2.1— and the same process will be repeated successively.

7. When any of the stopping requirements is satisfied, the overall identification will be terminated and an ultimate cleaning of spurious poles will be conducted among the final ones.

We present in Figure 3.2 a flow diagram to summarize the created automatic identification algorithm[2].

---

[2]The add-ons to the state-of-the-art algorithm are represented in orange boxes, whereas the usual elements are contained in yellow ones.
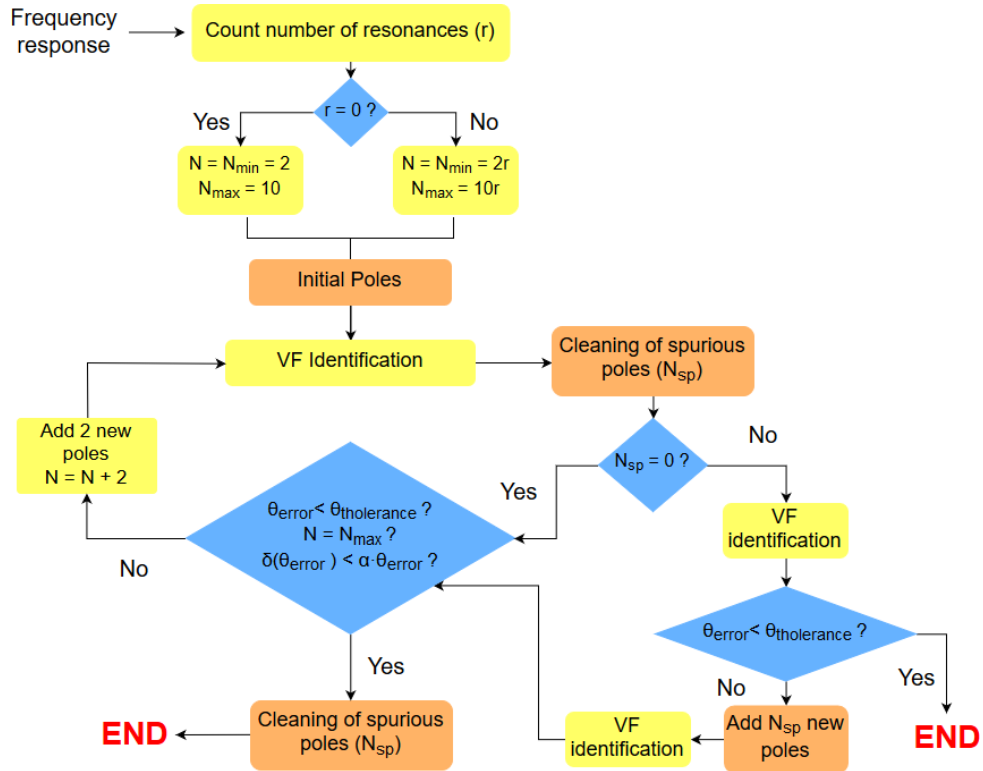
Figure 3.2: Flow diagram of the VF based automatic algorithm developed in this project.

The entire algorithm has been implemented in *Matlab* under the name of *main_stab*, using the Vector Fitting package developed by Bjørn Gustavsen [16]-[18]. In the main interface, presented in Figure 3.3, the user can choose the values of the different parameters to conduct the automatic identification.
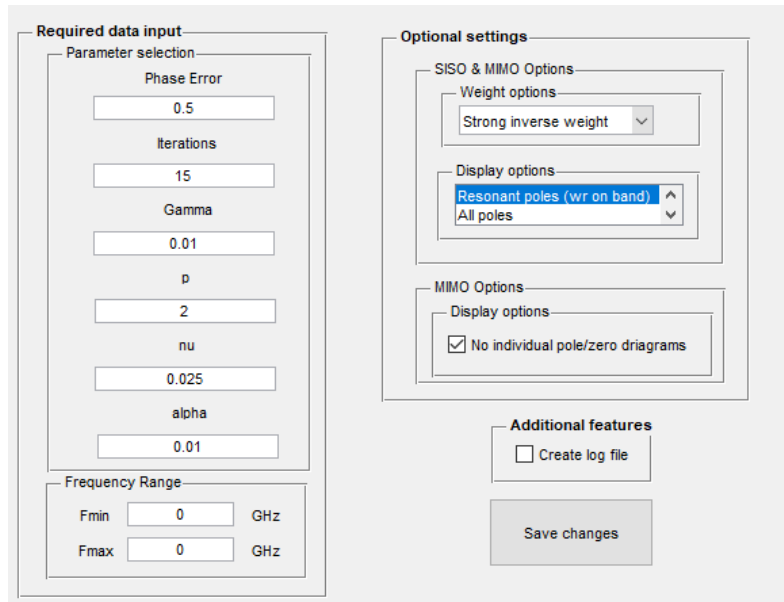

Figure 3.3: Capture of the initial interface of the created tool.

After several tests we suggest the following setting to use by default:

- Number of iterations: $N_{iter} = 15$.

- P-norm parameter: $p = 2$.

- Spurious poles discriminator: $\gamma = 0.01$.

- Phase tolerance: $\theta_{tolerance} = 0.5$

- Minimum distance delimiter: $\nu = 0.01$.

- Error variation threshold: $\alpha = 0.001$.

Nevertheless, it is interesting to point out that setting $\gamma = 0$, $\nu = 0$ and $\alpha = 0$, we recover the state-of-the-art automatic VF identification algorithm, same one as in Section 3.1.

Furthermore, as a supplement, the created tool offers the opportunity to visualize the last result *before* and *after* the last cleaning of spurious poles, as shown in Figures 3.4 and 3.5. If no spurious poles are found a single pop-up window will appear.
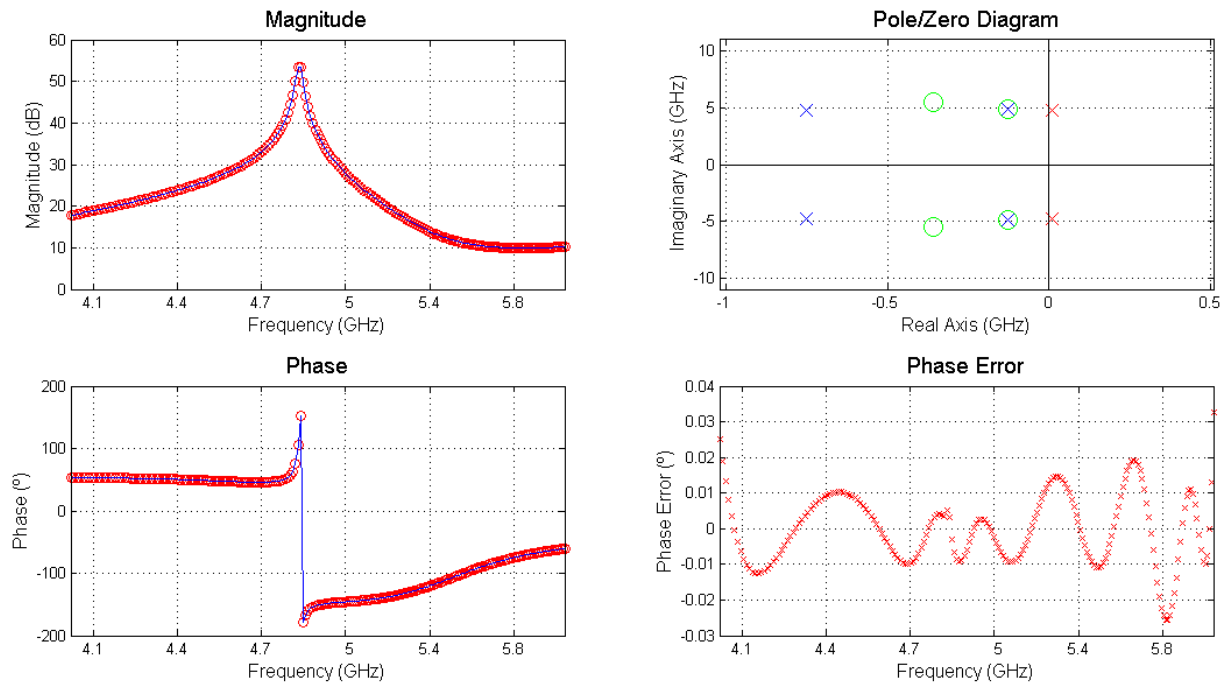
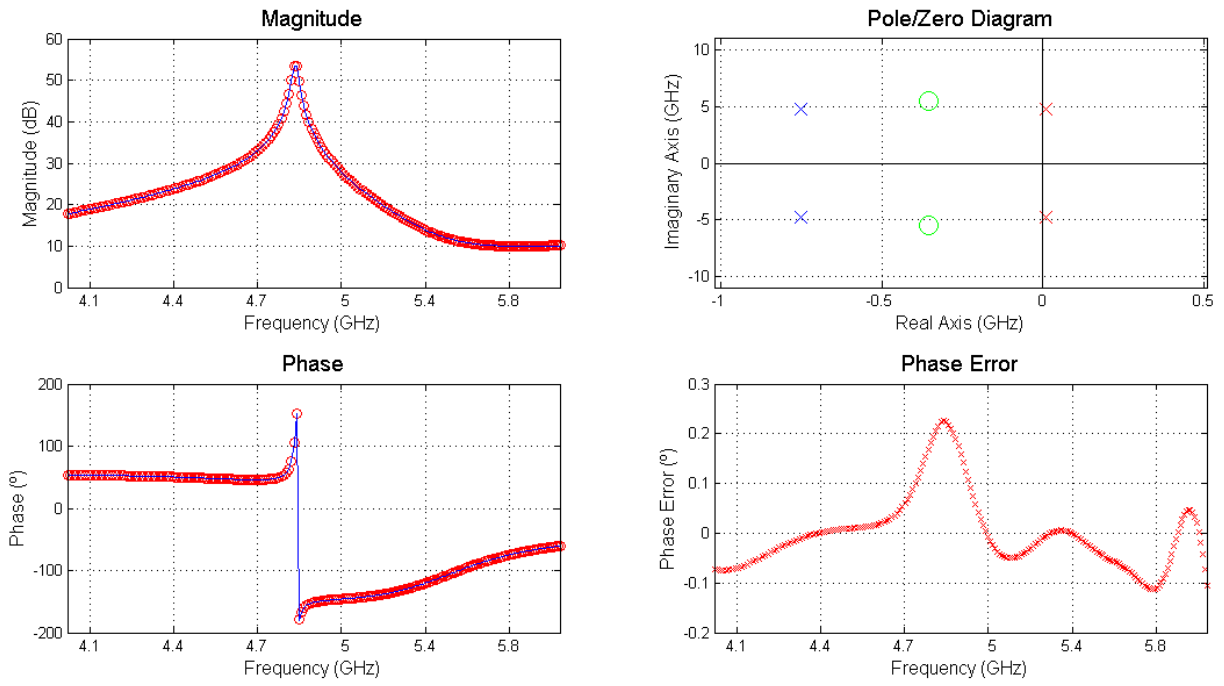Figure 3.4: Result of the automatic identification *before* the cleaning of spurious poles.

Figure 3.5: Result of the automatic identification *after* the cleaning of spurious poles.

Chapter 4

Comparative Analysis of the Two Automatic Vector Fitting Identification Algorithms

In this chapter we will perform an automatic Vector Fitting Identification with each of the methods explained in Chapter 3 on several frequency responses. We will then compare those results and try to extract the possible advantages and drawbacks of our proposed method (see Section 3.2), mainly regarding over-modeling, the main issue tackled in this project.

4.1   Analytical Frequency Responses with Added Gaussian Noise

First of all, to ensure the validity of our algorithm and provide a more reliable comparison, we have created a set of transfer functions in *Matlab* to serve as a reference, choosing manually the position of their poles, their zeros and the gain. Knowing the actual result of the identifications, we will be able to discern for each case the finest fitting between the two methods and, furthermore, estimate their limitations.

To generate this set, we have started by creating 4 different transfer functions with the same poles but different zeros. They all have a quasi-cancellation between a pole and a zero, *i.e.*, they all have a complex conjugate couple of pole-zeros placed very close in the complex plane. In fact, the only characteristic differentiating one transfer function from the other is that distance. Thus, we have created 4 distinct samples of the same transfer function, each with a particular level of pole-zero quasi-cancellation. Then, we have added different levels of Gaussian noise to these 4 samples (option provided by *Matlab*) to hinder the identification of the transfer functions.

Due to the limited length of this report, after analyzing a vast quantity of the generated frequency responses, we will only present the most illustrative and significant results, that are the extreme situations. Therefore, we will examine a very noisy and a barely noisy frequency response for both the set with the weakest pole-zero quasi-cancellation (first set) and the set with the strongest one (second set). That way, we will be able to study how these automatic VF identification algorithms respond in the event of physical quasi-cancellations (not numerical), noise and a combination of them.

The ideal identification —if noise were not fitted— should provide the same result for both responses of the same set, as they only differ in their level of Gaussian noise. The exact pole-zero maps for set 1 and

set 2 are depicted in Figures 4.1 and 4.2 respectively[1]. In addition, these maps show clearly the different level of pole-zero quasi-cancellation between the first set and the second one.
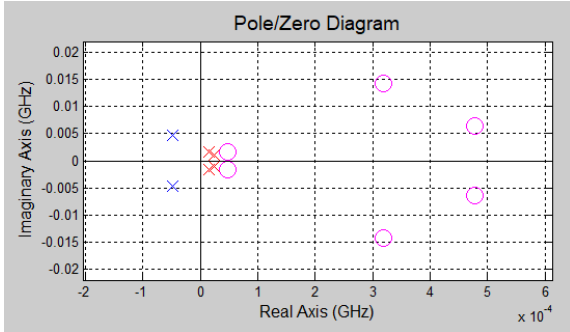

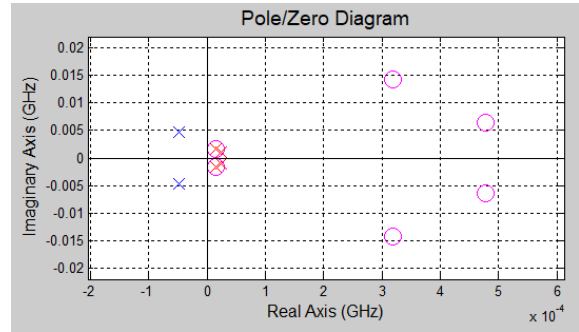Figure 4.1: Exact poles and zeros of Set 1. Order of the transfer function $N = 6$.

Figure 4.2: Exact poles and zeros of Set 2. Order of the transfer function $N = 6$.

Before the beginning of the comparative analysis, it must be pointed out that all the identifications will be carried out with the default settings fixed in Subsection 3.2.2.

Among those parameters, it must be emphasized that the phase tolerance $\theta_{tolerance}$ will determine to a large extent the results obtained in the analysis of the different frequency responses. In particular, the default value $\theta_{tolerance} = 0.5º$ might be troublesome when identifying the frequency responses of Set 2, as the phase shift due to the quasi-canceled pole is of approximately 0.4º.

Case 1a:

If we perform the automatic identification on the noisiest response of the first set, Case 1a, a substantial number of quasi-canceled poles and zeros is obtained in the pole-zero map of Figure 4.1 (the exact result if noise were not fitted). For instance, if we perform the automatic identification with the mentioned *MM_stab* (see Section 3.1), we obtain a large amount of spurious poles, as shown in Figure 4.3. In fact, the order of the identified transfer function is 6 times the actual one: $N_{identified} = 36$ and $N = 6$.

Likewise, if we perform the same identification with our algorithm *main_stab* (with default parameters), we also obtain a substantial number of spurious poles *before* the last cleaning, as presented in Figure 4.4. Specifically, we obtain a transfer function of order $N_{identified} = 32$, whereas if noise were not fitted, we should ideally obtain $N = 6$.

However, after the last cleaning, all these quasi-canceled poles and zeros are suppressed and we obtain the expected poles, as shown in Figure 4.5. From the same figure, one can also remark that the fitting error is considerably increased and that the fitting goal $\theta_{tolerance} = 0.5º$ is no longer achieved. This is mainly due to the difference in the zeros; they are less resonant and correspond to a region of high frequency where the magnitude is lower and, hence, more sensitive to the noise. Still, it must be kept in mind that it is an identification of a noisy response[2] and that our algorithm has been able to identify *no more and no less* than the actual poles, an indispensable condition for a proper stability analysis.

---

[1]Poles are represented by 'X'-s and zeros by 'O'-s.
[2]When trying to fit a noisy response it is suggested to relax the fitting goal by increasing the phase tolerance.

14

In addition, as it will be later detailed, the maximum phase error obtained *after* the last cleaning of spurious poles can serve as a warning of the presence of noise and to suggest a less strict $\theta_{tolerance}$.
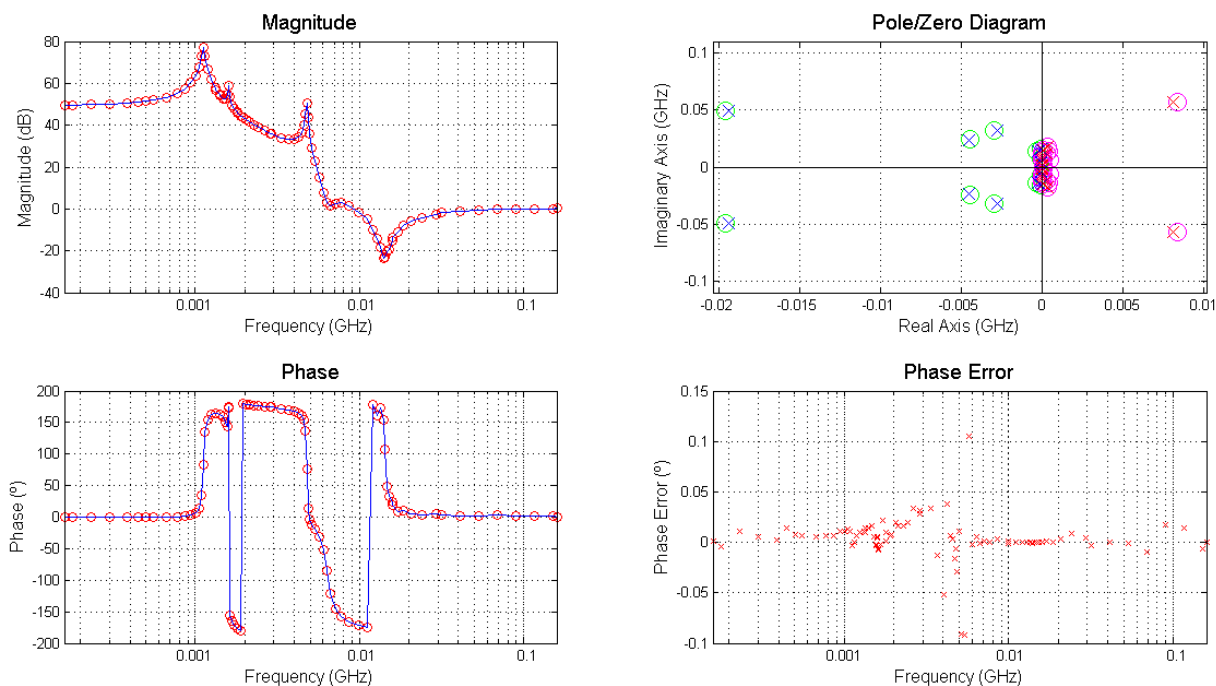

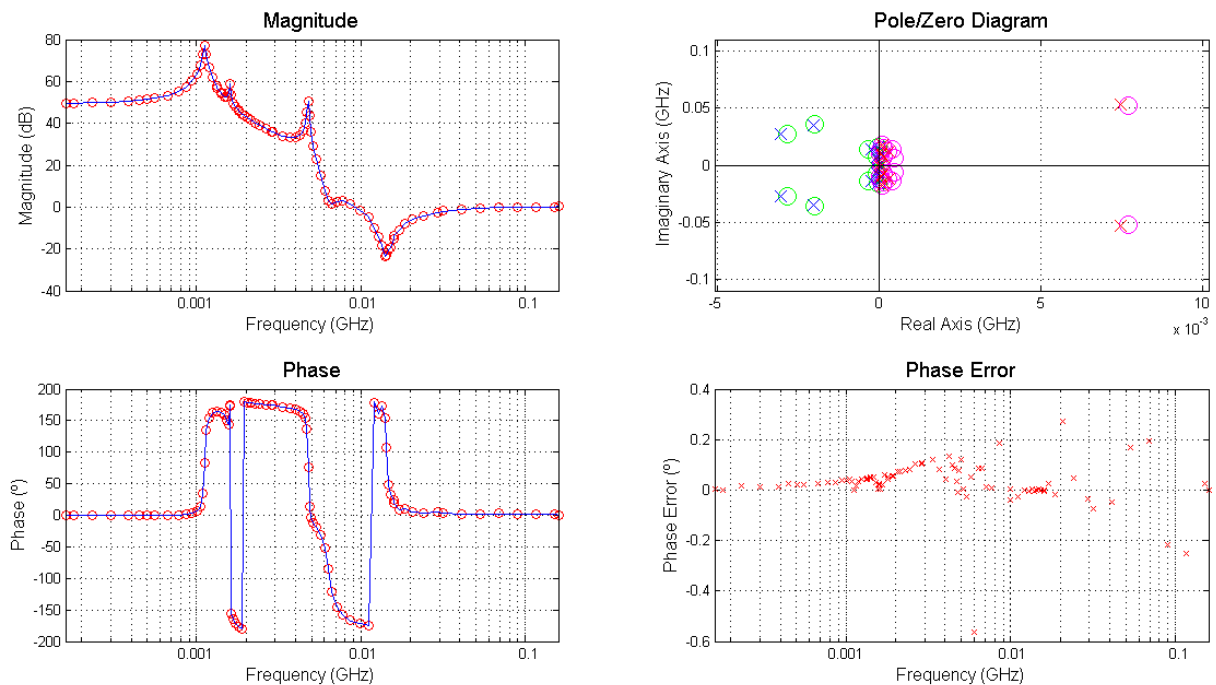Figure 4.3: Result of the identification of Case 1a with *MM_stab*. $N_{identified} = 36$.

Figure 4.4: Result of the identification of Case 1a with our tool *before* the last cleaning of spurious poles. $N_{identified} = 32$.
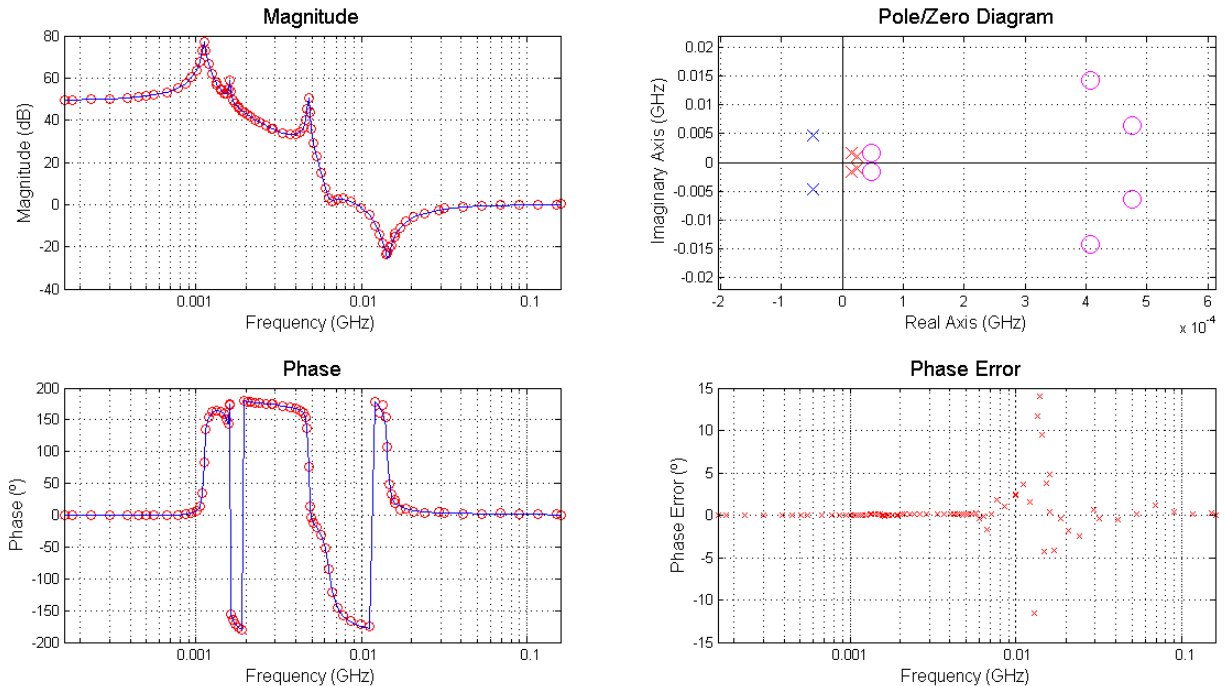
15

Figure 4.5: Result of the identification of Case 1a with our tool *after* the last cleaning of spurious poles. $N_{identified} = 6$.

Case 1b:

If we carry out the identification of a less noisier response of the first set, Case 1b, we notice that over-modeling is drastically diminished with either of the methods. This can be seen from Figures 4.6 and 4.7, where the result of the identification with *MM_stab* and our tool *before* the last cleaning of spurious poles are depicted, respectively. Hence, in this case, the enhancements of our algorithm are not that obvious, as both methods provide similar results. Nevertheless, even before the last cleaning of spurious poles, we remark from these same figures that our algorithm fits the response with a lower order than *MM_stab*, all respecting the phase tolerance.

Indeed, in both cases the iteration loop has been stopped once the phase tolerance has been reached, but thanks to the novel placing of the added poles, our algorithm has been able to reach this goal by fitting the noisy response with a lower order. Thus, we can already state that even before the last cleaning, our automatic algorithm can decrease over-modeling due to a more appropriate placing of the poles (see Subsection 3.2.1).

Moreover, after the last cleaning, just as with the noisier response, all the spurious poles are suppressed, as seen in Figure 4.8. It must be noted that after the elimination, the fitting goal is no longer respected. Still, $\theta_{error} \approx 1.5^o$ is a coherent fitting error for a noisy response, since a lower one would fit the noise.

16
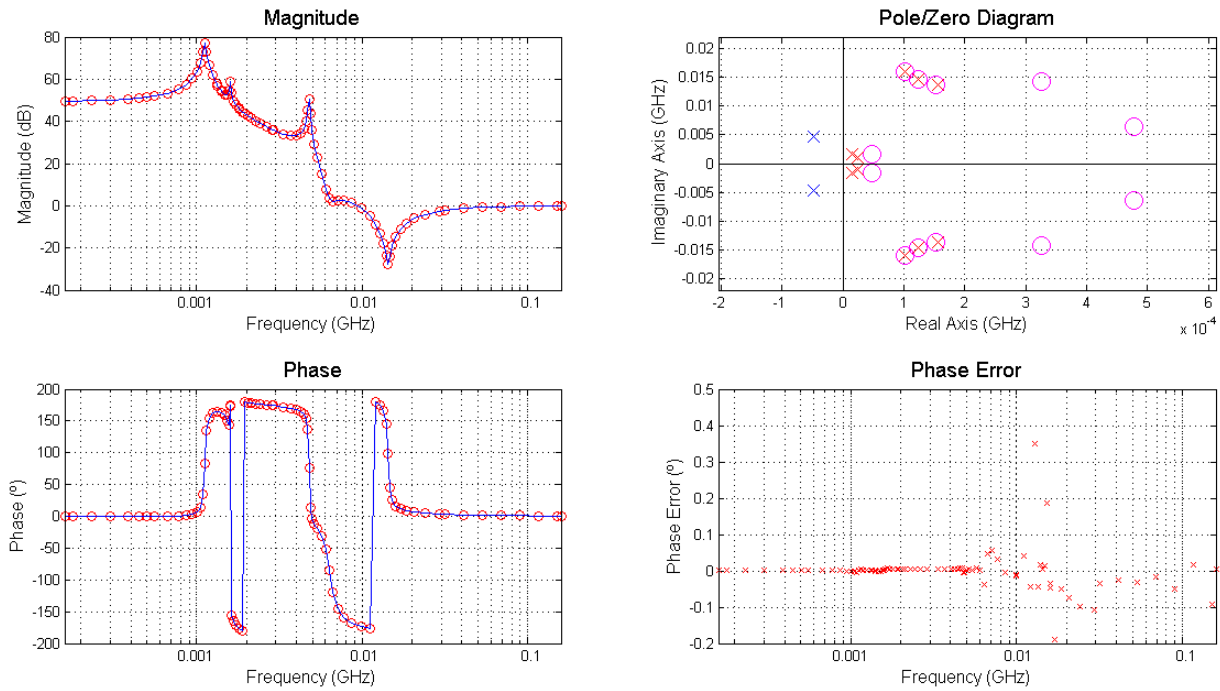
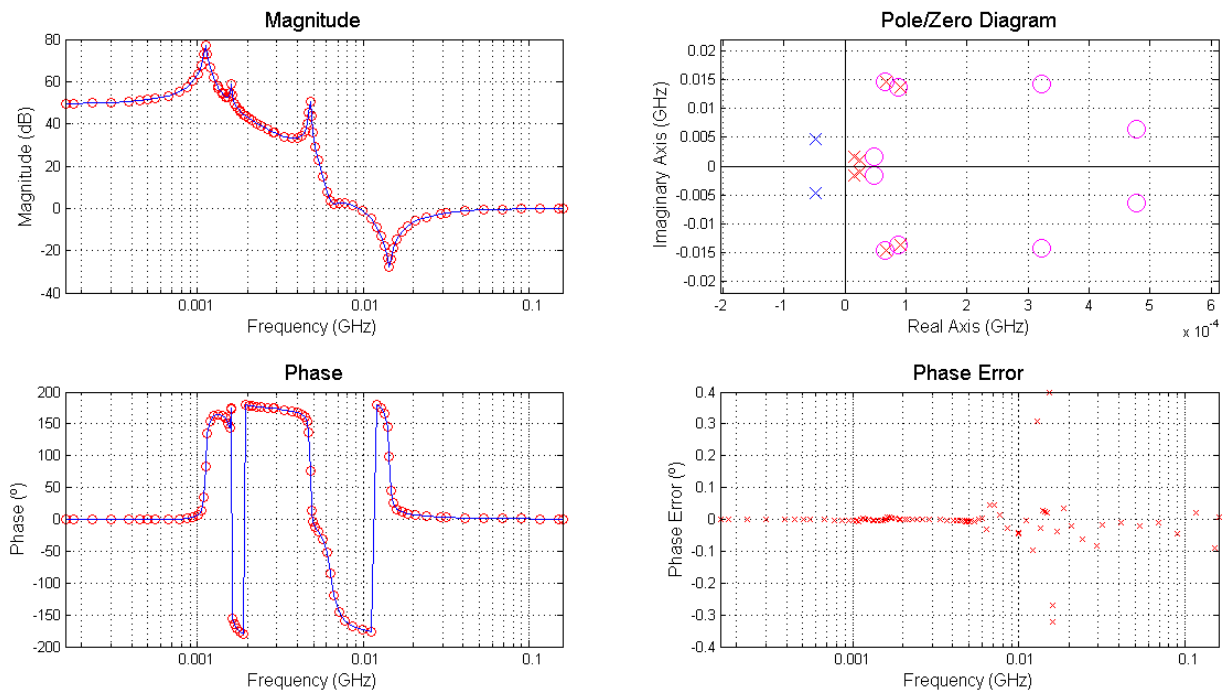Figure 4.6: Result of the identification of Case 1b with *MM_stab*. $N_{identified} = 12$.

Figure 4.7: Result of the identification of Case 1b with our tool *before* the last cleaning of spurious poles. $N_{identified} = 10$.

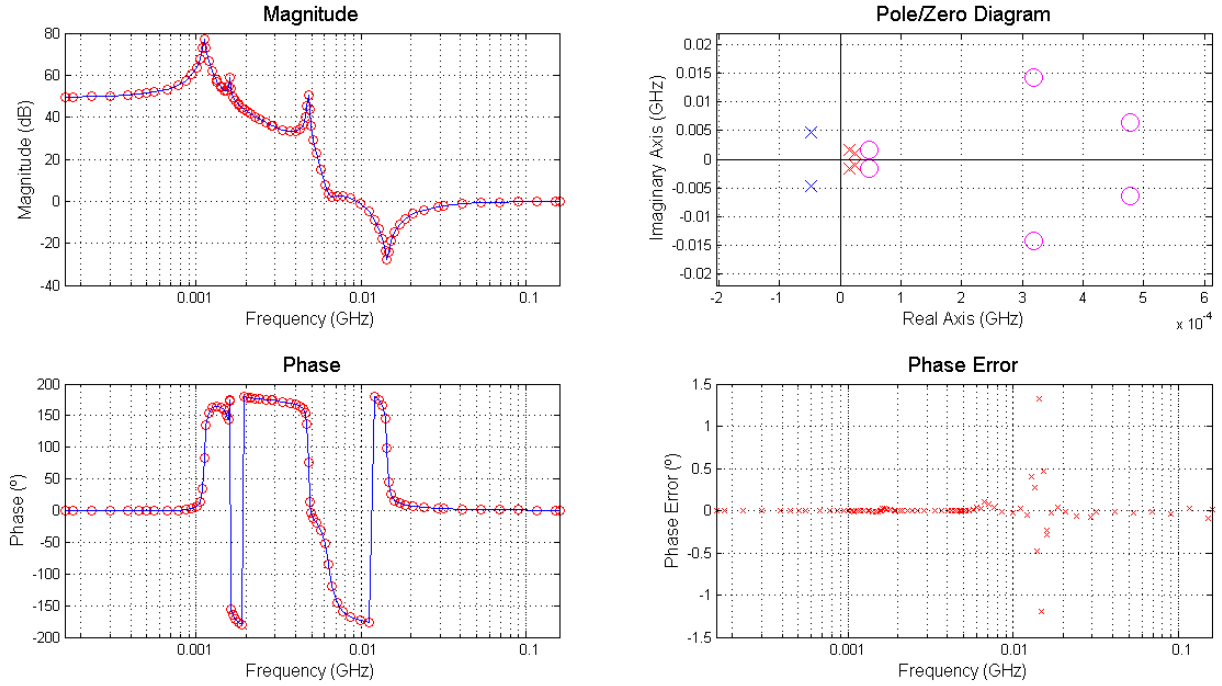Figure 4.8: Result of the identification of Case 1b with our tool *after* the last cleaning of spurious poles. $N_{identified} = 6$.

Case 2a:

We then continue with the set of transfer functions with the strongest quasi-cancellation, the second set. If we perform the automatic identification to a very noisy frequency response of this set, Case 2a, the fitted models are strongly over-modeled, similarly to Case 1a. This can be seen from Figures 4.9 and 4.10, where the identification carried out with *MM_stab* and by our tool *before* the last cleaning of spurious poles are respectively depicted.

The quasi-cancellation between the pole and the zero being so strong (see Figure 4.2) and the Gaussian noise so high, it is hardly detected by neither of the methods. Certainly, due to over-modeling, there is a large amount of poles and zeros near that region; therefore, it is difficult to state whether the *actual* quasi-canceled pole has been detected or whether it is "hidden" inside the noise. Nonetheless, some other valuable remarks and conclusions can be drawn regarding the differences between the two algorithms. For instance, we can notice that the identification carried out by our algorithm does not meet the fitting goal, as $\theta_{error} \approx 2.5^{\circ}$. In fact, the iteration process has been stopped due to the implemented novel condition (3.2): the threshold error variation between successive iterations. As a consequence, the order of the fitted model is $N_{identified} = 30$, whereas the one obtained with *MM_stab* is 36. Indeed, even if both fitting models are extremely over-modeled, we can state that this extra condition can help, in a way, to mitigate the effect of our problem in hand.

On the other hand, *after* the last cleaning of spurious poles, we obtain the result presented in Figure 4.11. As before, all of the spurious poles have been eliminated, even seemingly the quasi-canceled pole and zero or, at least, the large amount of quasi-canceled poles near it.
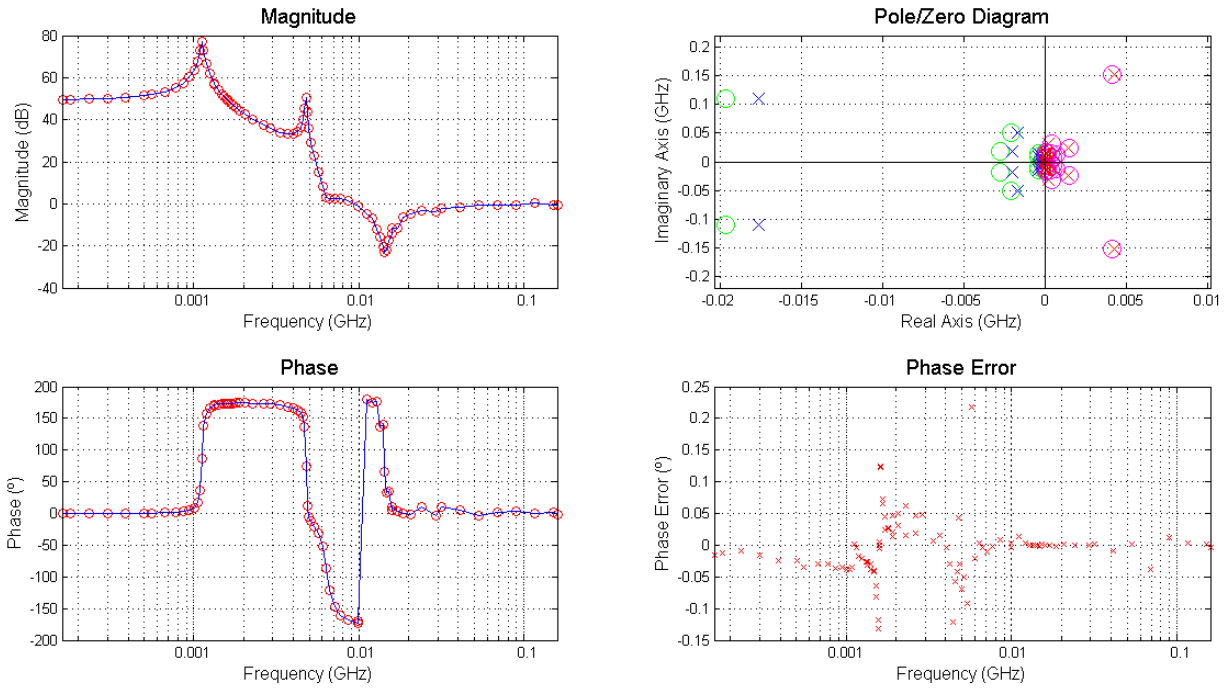
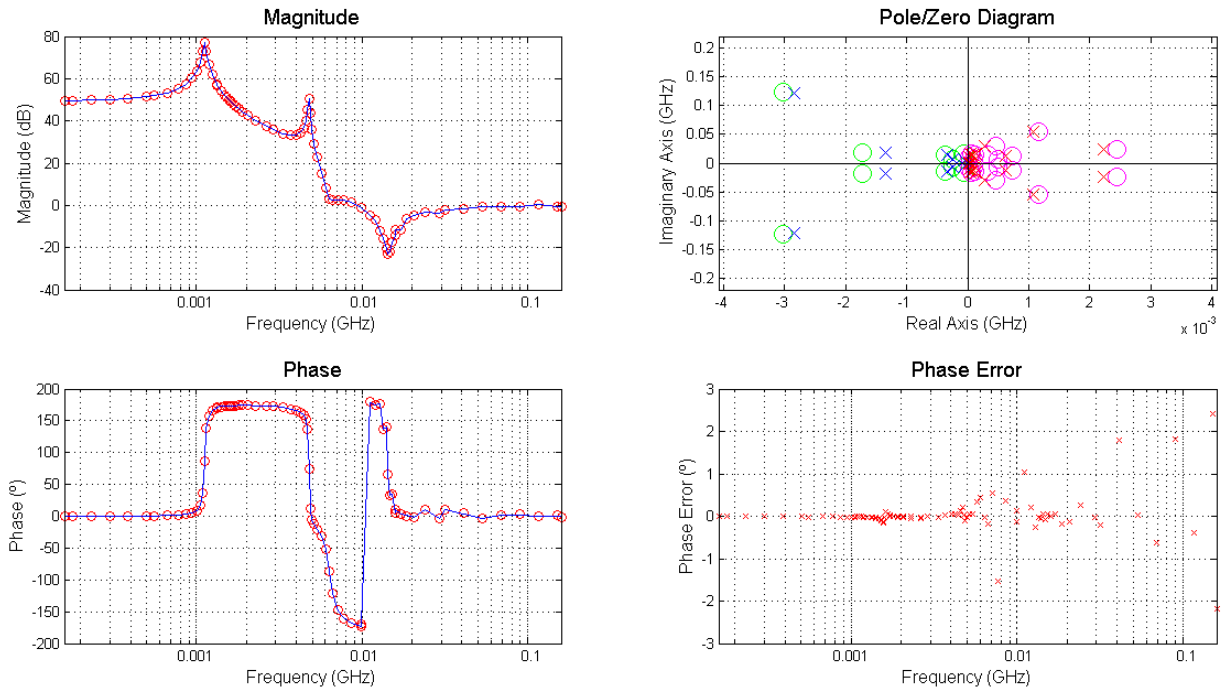Figure 4.9: Result of the identification of Case 2a with *MM_stab*. $N_{identified} = 36$.

Figure 4.10: Result of the identification of Case 2a with our tool *before* the last cleaning of spurious poles. $N_{identified} = 30$.
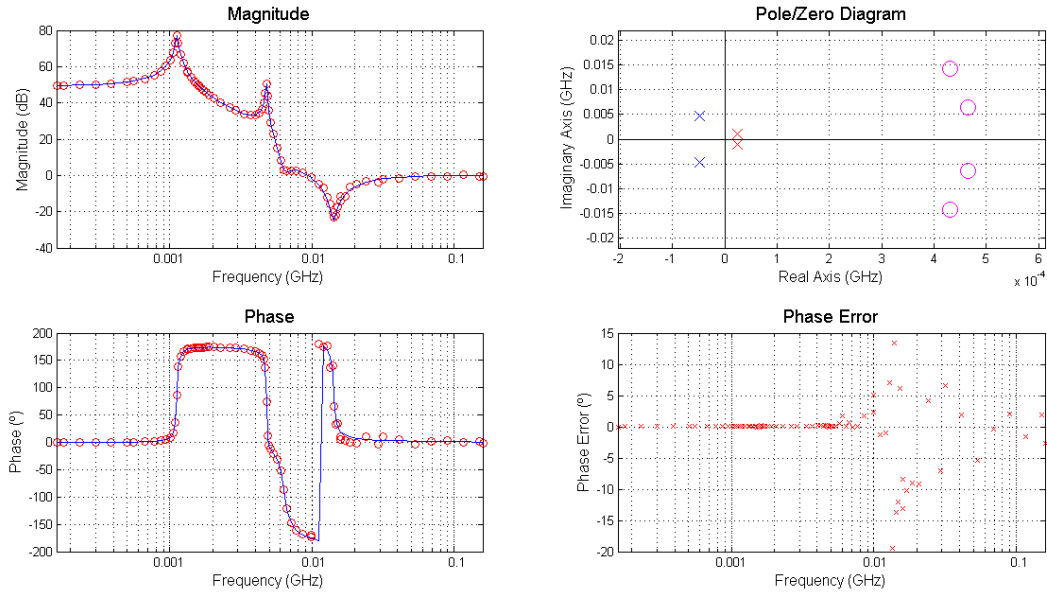
Figure 4.11: Result of the identification of Case 2a with out tool *after* the last cleaning of spurious poles. $N_{identified} = 4$.

Case 2b:

If we carry out the identification of a less noisier response of this same set, Case 2b, we first notice that the number of spurious poles is greatly reduced with either methods. This can be seen from Figures 4.12 and 4.13, where the identification carried out with *MM_stab* and by our algorithm *before* the last cleaning of spurious poles are depicted, respectively. Moreover, from these same figures, we can also observe that *before* the last cleaning of spurious poles, both identifications are identical.
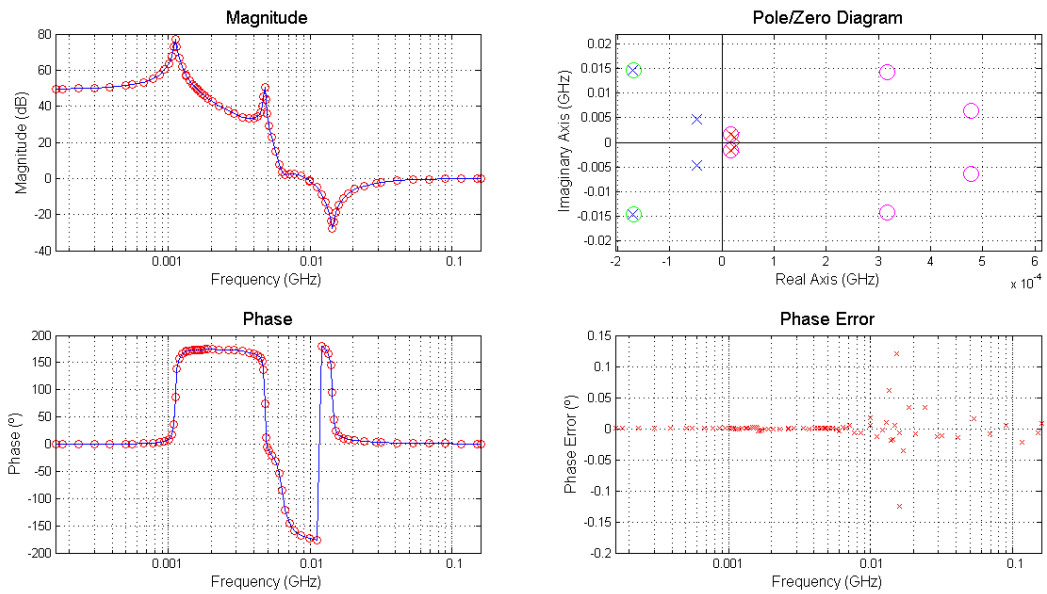

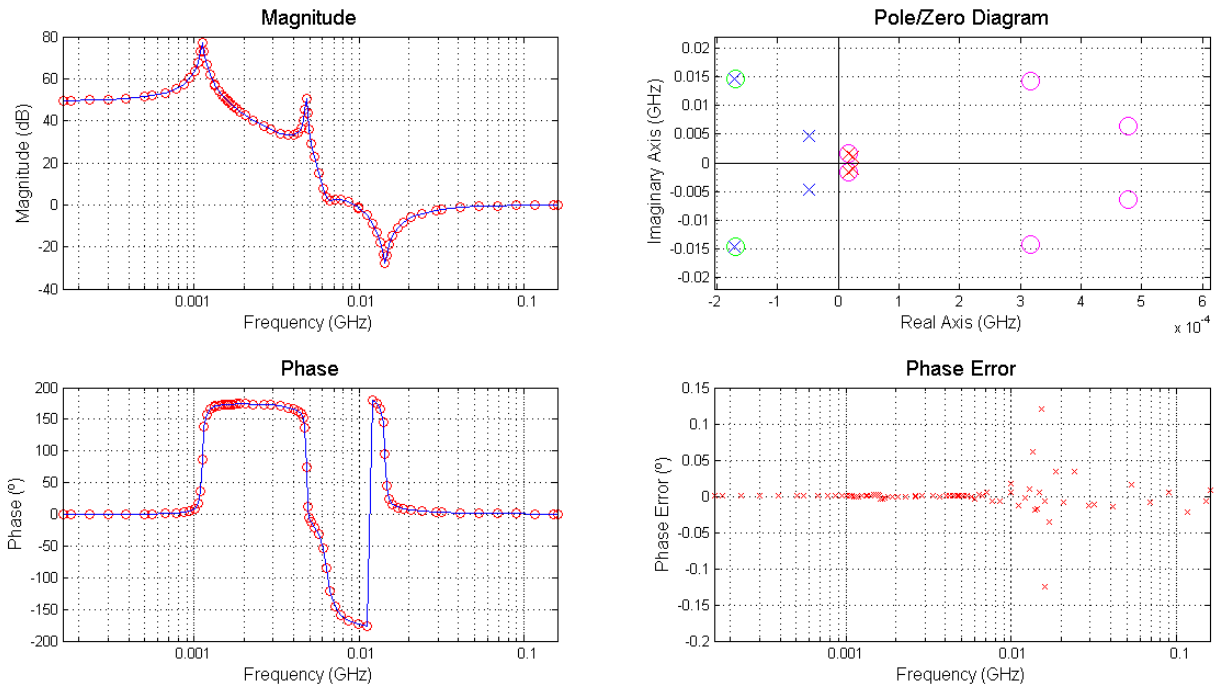Figure 4.12: Result of the identification of Case 2b with *MM_stab*. $N_{identified} = 8$.

Figure 4.13: Result of the identification of Case 2b with our tool *before* the last cleaning of spurious poles. $N_{identified} = 8$.
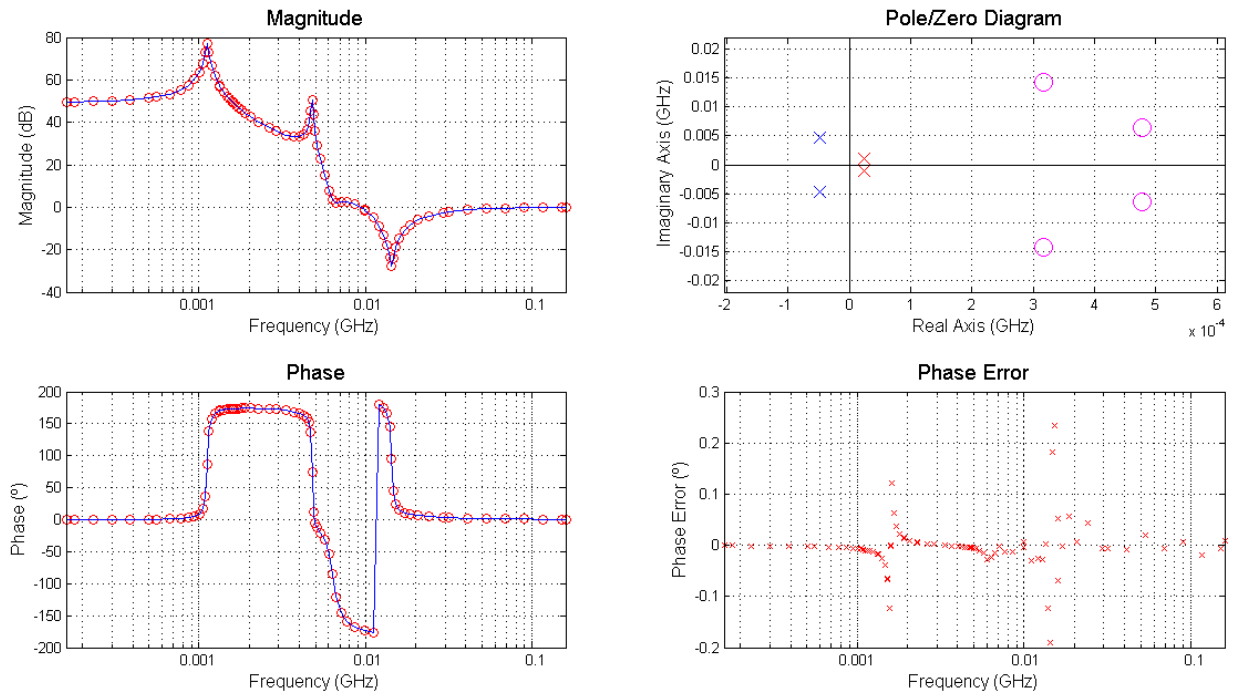

Figure 4.14: Result of the identification of Case 2b with our tool *after* the last cleaning of spurious poles. $N_{identified} = 4$.

Having reduced the noise level, significantly fewer poles are detected compared to Case 2a. Precisely, *before* the last cleaning of spurious poles only 8 poles are identified: all the original 6 plus another 2 quasi-canceled. Nonetheless, *after* the last cleaning of spurious poles, the *numerical* quasi-cancellation is removed alongside the *physical* one, as showed in Figure 4.14. After this removal, as it can be observed from this last figure, the phase error has increased just up to 0.25°, which is coherent with the fact that the phase shift produced by the physical quasi-cancellation is lower than 0.5°.

In fact, when a pole and a zero are extremely close, as in this case, our algorithm is not able to distinguish a physical quasi-cancellation of that kind from a *numerical* one; they both make a negligible contribution to the total transfer function and therefore they are both equally dispensable. However, if we make our algorithm display the d_n factor (presented in Subsection 3.2.2) of this pole, we observe that it is of the order of 10^{-4}, whereas the one relative to the spurious pole is of the order of 10^{-7}. In other words, the physical quasi-cancellation has a d_n factor several orders of magnitude greater than the numerical one: $10^{-4} \gg 10^{-7}$.

Consequently, when a similar situation is encountered —when the nature of a quasi-cancellation is uncertain— we can make our algorithm display the values of d_n for all the quasi-canceled poles and check whether it is of several orders of magnitude greater for this pole than for the other ones. In such event, we can consider it to be physical, assuming that the noise is lower than this presumed physical quasi-cancellation.

Before bringing this analysis to a conclusion, we will make a brief digression regarding the effect of the chosen phase tolerance for both algorithms. It must be emphasized that all of the identifications have been carried out with the default settings of both algorithms; parameters that have been carefully chosen in order to guarantee convergence and reduce over-modeling. However, what would be the effect of changing those values? Specially, phase tolerance is the most sensitive one.

In the event of a really high phase tolerance, the fitting model might be under-modeled, *i.e.*, part of the dynamics will be missing. On the other hand, if a very low phase tolerance is requested, the fitting model might be over-modeled and too many parameters will be added, for instance, the fitting of the noise. Nevertheless, finding a middle ground can be complex and sometimes, even impossible. In fact, even though $\theta_{tolerance}$ is set by default to 0.5° for both algorithms, it might not be adequate for the frequency response under study[3].

With the state-of-the-art algorithm, the most suitable value of $\theta_{tolerance}$ for a certain type of frequency response is to be found in a slightly intuitive way, mainly by trial-error. This can be tricky for designers, as they might not have an in-depth knowledge of identification methods. Conversely, the last fitting error of our algorithm —*after* the last cleaning of spurious poles— provides an estimated value of the most suitable $\theta_{tolerance}$ for frequency responses of the same kind. Indeed, due to the extra stopping condition (3.2) and the last cleaning of spurious poles, the final phase error must not satisfy the phase tolerance and as a consequence, its maximum value can be taken as an estimator of a $\theta_{tolerance}$ coherent with that level and type of noise. As an example, from Figure 4.5 we can consider that the most reasonable value of $\theta_{tolerance}$ for that certain type of frequency responses is 15°, instead of the default value 0.5°.

This is certainly observed in Figures 4.15 and 4.16, where the identification of Case 1a has been carried out for $\theta_{tolerance} = 15°$. Before the last cleaning of spurious poles, a single numerical quasi-cancellation is observed, which, in addition, is stable. Besides, the identification order is significantly reduced from $N_{identified} = 32$ to $N_{identified} = 8$. Moreover, after the last cleaning of spurious poles (Figure 4.16), this complex conjugate couple of quasi-canceled pole-zeros is suppressed and we obtain the same result of Figure 4.5.

---

[3]Adequate in the sense of avoiding *both* under-modeling and over-modeling.
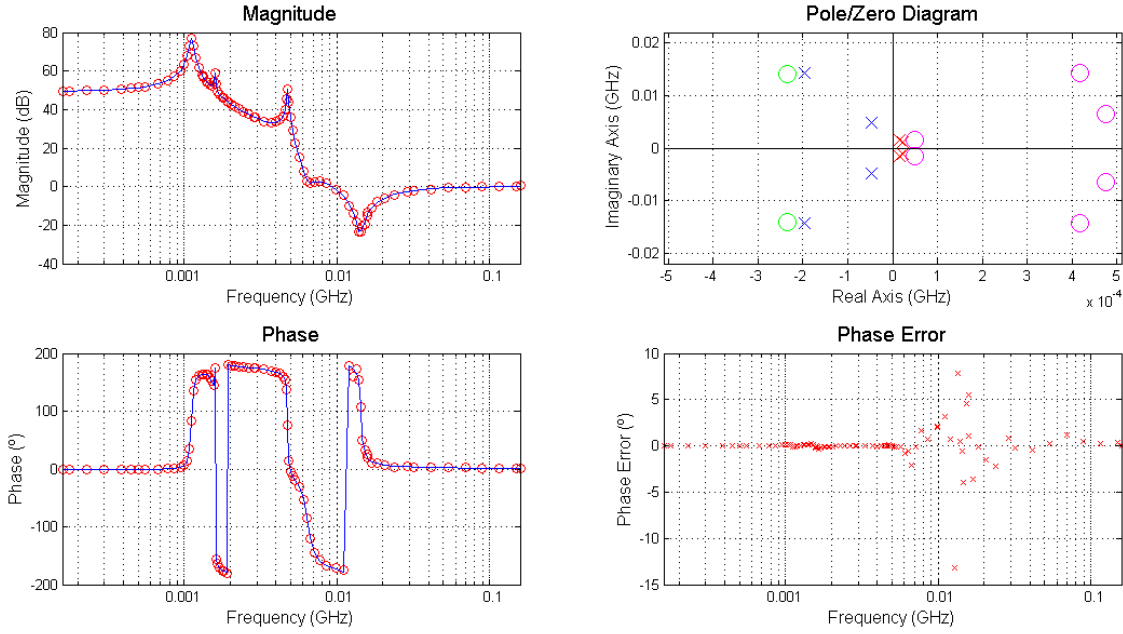
Figure 4.15: Result of the identification of Case 1a with our tool and $\theta_{tolerance} = 15°$ *before* the last cleaning of spurious poles. $N_{identified} = 8$.
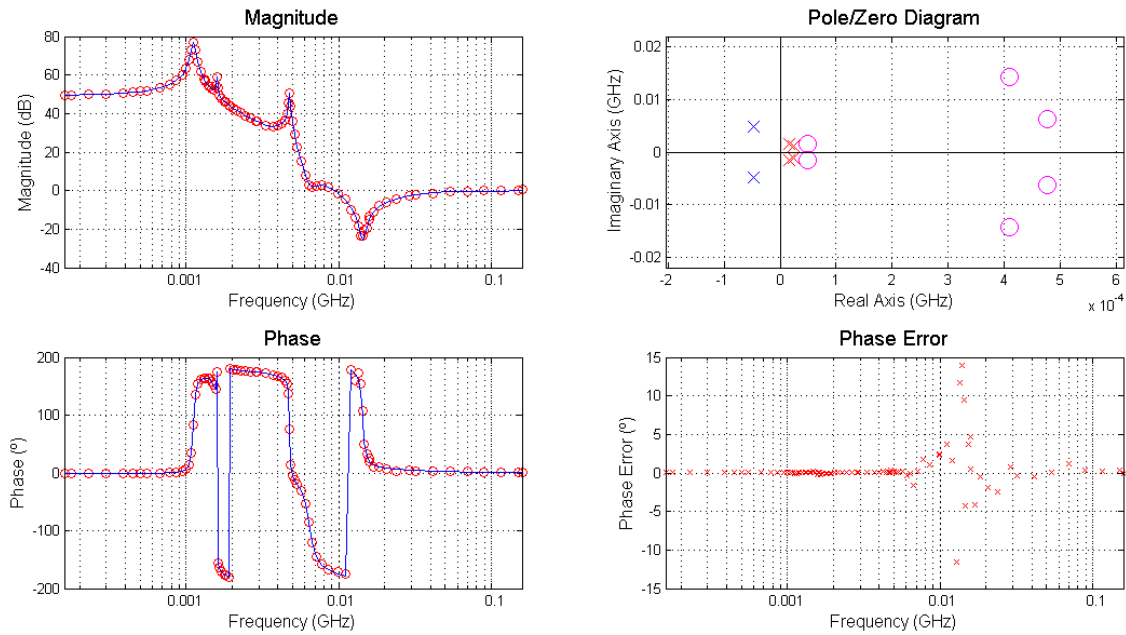

Figure 4.16: Result of the identification of Case 1a with our tool and $\theta_{tolerance} = 15°$ *after* the last cleaning of spurious poles. $N_{identified} = 6$.

Finally, to conclude this section, we can state that these identifications have revealed the main problems encountered with noisy frequency responses and strong physical quasi-cancellations, but specially, when these quasi-cancellations become imperceptible inside the noise.

With regards to the possible improvements introduced by our algorithm, first of all, we have confirmed the crucial role of the last cleaning regarding the suppression of spurious poles in the event of noise.

23

Furthermore, we have also observed that both the novel placing of the poles introduced in Subsection 3.2.1 and the stopping condition (3.2) contribute to reduce over-modeling, as deduced when comparing the identified orders in *MM_stab* and our algorithm *before* the last cleaning.

On the other hand, we have also detected the limitations encountered by both methods when a highly noisy response contains a strong physical quasi-cancellation. As formerly mentioned, in that event, neither of the methods is able to detect clearly the couple of quasi-canceled pole-zeros. However, even if they are indeed detected, due to the almost negligible distance between the pole and the zero, they are suppressed during the last cleaning introduced in our algorithm. That is, our tool struggles to distinguish a strong physical quasi-cancellation from a numerical one.

Accordingly, as mentioned, we suggest for our algorithm to compare the d_n factors of the quasi-canceled poles. Indeed, a single SISO response has limited resources to differentiate a *physical* quasi-cancellation from a *numerical* one. Ideally, we should perform a MIMO or a parametric analysis, to see whether that pole is clearly detected in another node or whether it follows a deterministic path versus a relevant circuit parameter.

4.2   Realistic Frequency Responses of RF Amplifiers

In the former section, we have made a comparative analysis of the two algorithms for analytical frequency responses with Gaussian noise. However, frequency responses of RF amplifiers are of a different nature; they correspond to a linearized steady state and are generally obtained from a numerical simulation or, in some cases, from experimental characterization. Therefore, they are much more complex and challenging to identify.

Hence, in order to verify the validity of our algorithm for the stability analysis of RF and microwave amplifiers, in this last section we will analyze realistic frequency responses of a RF amplifier, obtained both by numerical simulations and experimental characterization. The device under test (DUT) is a hybrid L-band three-stage amplifier built in microstrip technology and based on GaAs FET transistors (FLU17XM). Its picture and schematic are depicted in Figures 4.17 and 4.18 respectively.
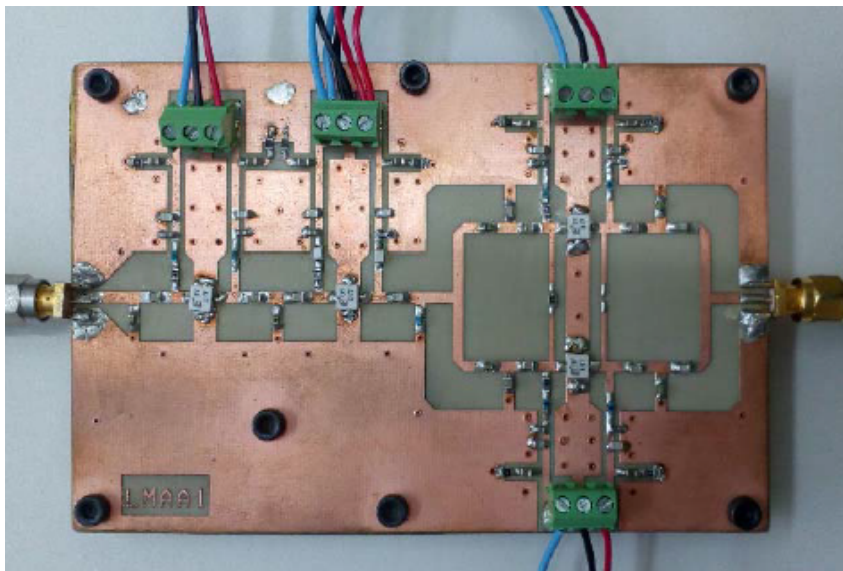

Figure 4.17: Photograph of the GaAs FET-based L-band three-stage amplifier in microstrip technology. Figure obtained from [21].
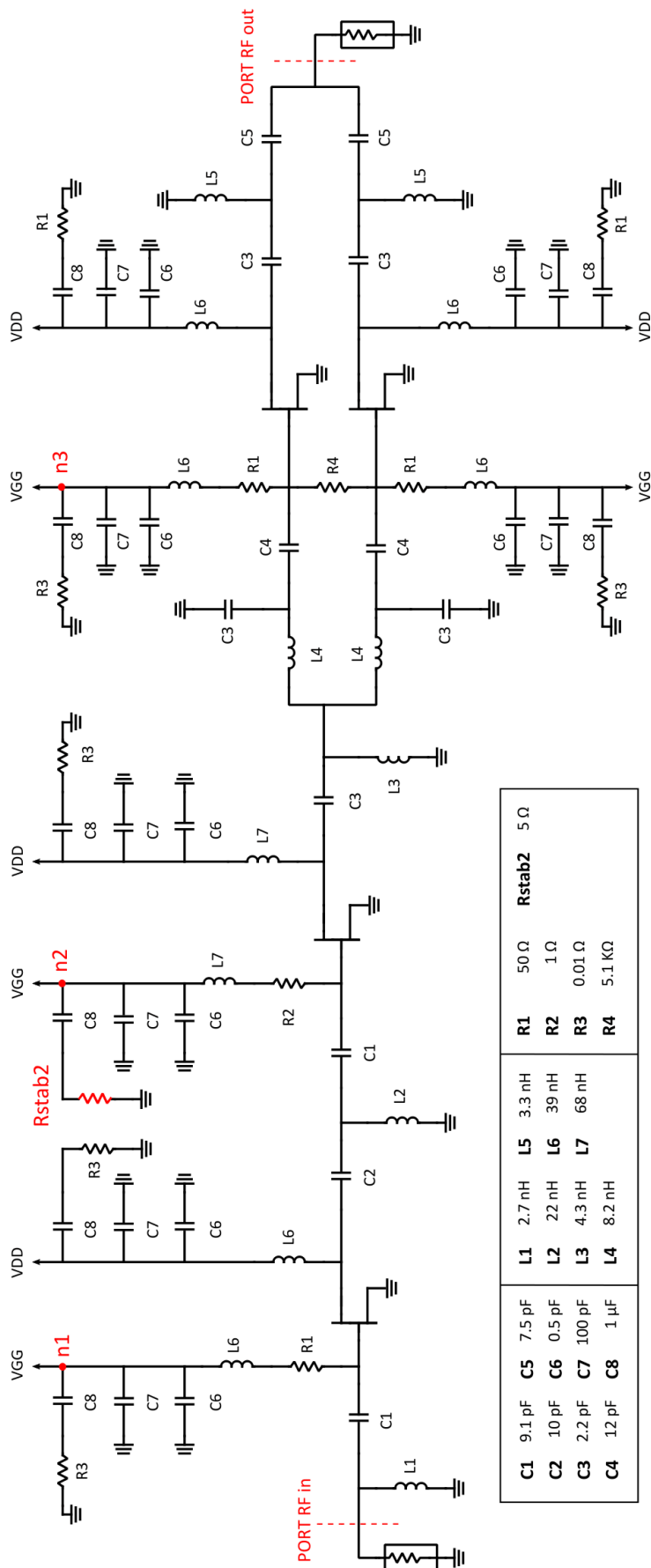
Figure 4.18: Schematic of the L-band three-stage amplifier of Figure 4.17. Figure obtained from [21].

With a pumping signal of $f_0 = 1.2\,\text{GHz}$ and biased at $V_{GG} = -2.1\,\text{V}$ and $V_{DD} = 7\,\text{V}$, the amplifier presents a low frequency oscillation for input powers greater than $P_{in} > -11\,\text{dBm}$ [21]. This is clearly shown in Figure 4.19, where the measured output power spectrum is depicted for $P_{in} = -5\,\text{dBm}$. This spectrum shows mixing terms of type $mf_0 \pm nf_s$ ($m, n \in \mathbb{N}$), where $f_s \approx 135\,\text{MHz}$ is the frequency of the oscillation.
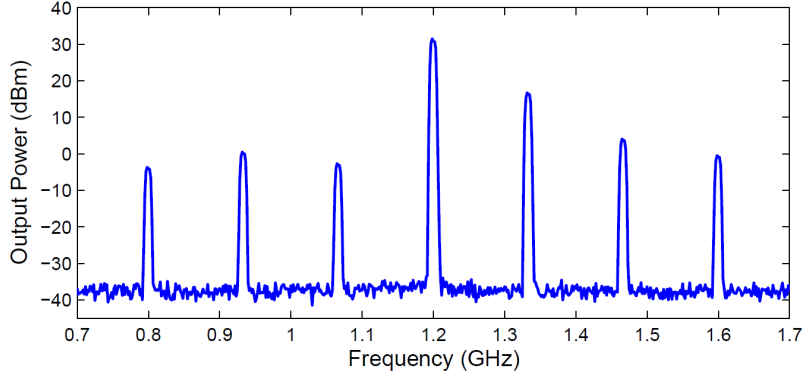

Figure 4.19: Measured output power spectrum showing the mixing terms around $f_0 = 1.2\,\text{GHz}$ for $P_{in} = -5\,\text{dBm}$.

This instability is due to a pair of complex conjugate poles with an imaginary part of $f_s \approx 135\,\text{MHz}$ and a shifting real part versus the input power P_{in}. In fact, this evolution is depicted in Figure 4.20, obtained varying the input power from $-30\,\text{dBm}$ to $-5\,\text{dBm}$ [4]. From this figure, we observe that the real part of the pole shifts from negative to positive, causing the pole to become unstable for a certain threshold of input power, which confirms the instability found experimentally.
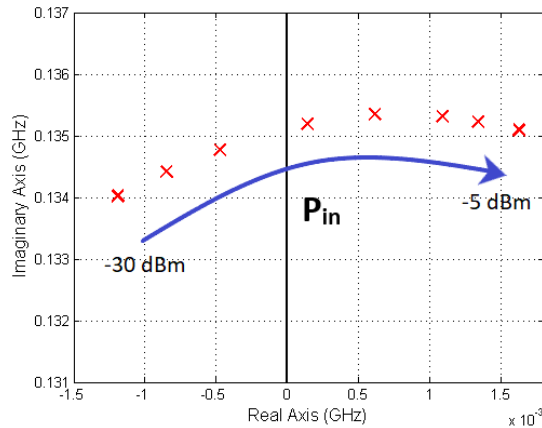

Figure 4.20: Evolution of the low frequency pole *vs.* the input power, with a pumping signal at $f_0 = 1.2\,\text{GHz}$ and biased at $V_{GG} = -2.1\,\text{V}$ and $V_{DD} = 7\,\text{V}$. For sake of clarity, only the positive frequencies (positive imaginary part) have been plotted.

This pair of complex conjugate poles is from the second stage [21], thus, it will be more clearly detected in the second stage. Likewise, quasi-canceled repetitions of this pair of poles (physical) appear at frequencies $mf_0 \pm f_s$ ($m \in \mathbb{N}$).

---

[4]This evolution has been computed with our algorithm performing an identification for each P_{in} value.

To begin to evaluate the validity and reliability of our algorithm for this type of amplifiers, we will proceed to identify several frequency responses with a non-zero input power P_{in} at $f_0 = 1.2\,GHz$ (for the mentioned bias point $V_{GG} = -2.1\,V$ and $V_{DD} = 7\,V$). These frequency responses correspond thus to a periodic large-signal steady state. Indeed, we know from [21] that we must obtain stable poles for $P_{in} < -11\,dBm$ and otherwise, a set of complex conjugate unstable poles with frequencies $mf_0 \pm f_s$ ($m \in \mathbb{N}$).

The frequency responses have been obtained introducing a current probe sequentially at the gate of each transistor (see Figure 4.18) and ranging the input power from $-30\,dBm$ to $-5\,dBm$. For all three nodes and input powers, every identification has shown the expected outcomes. Furthermore, we have not observed significant differences between the state-of-the-art algorithm and our own. Due to the limited length of this report, we can not present the totality of the results. However, we will show the results obtained for $P_{in} = 6\,dBm$ introducing a current probe at the gate of the transistor of the second stage and obtaining the impedance seen by the probe (see Section 2.1). The results of the automatic identification (with default settings) have been depicted in Figures 4.21 and 4.22, before and after the last cleaning of spurious poles, respectively.

From Figure 4.21, we observe that three unstable pairs of complex conjugate poles appear, with frequencies f_s and $f_0 \pm f_s$ as expected, two being quasi-canceled and one clear[5]. On the left-half-plane, however, we notice a large number of quasi-canceled poles and zeros; that is, the identification might be over-modeled.
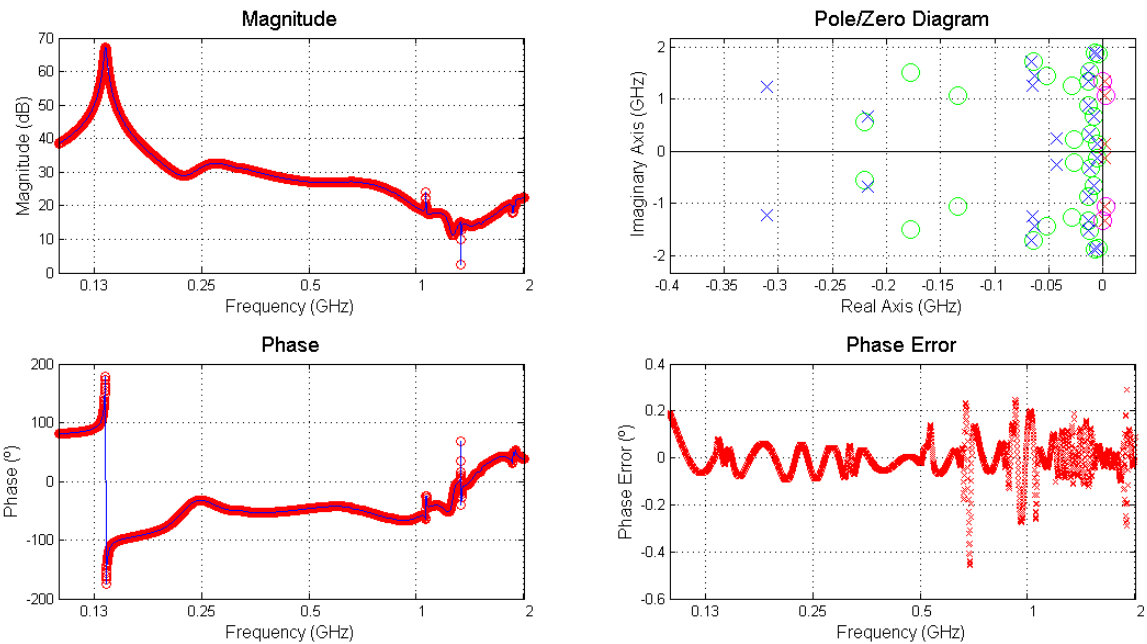

Figure 4.21: Identification results of the frequency response simulated in the second stage of the L-band amplifier with input power $P_{in} = -6\,dBm$, carried out by our algorithm and *before* the last cleaning.

From Figure 4.22 we notice that a considerable number of quasi-canceled pole-zeros are eliminated after the last cleaning, but specially, that the physical quasi-cancellation at frequencies $f_s \pm f_0$ are unaffected. Actually, the phase error has increased after this last step, nevertheless, considering the stable nature of the suppressed pole-zero quasi-cancellations, the conclusions regarding the stability are not altered.

---

[5]As previously stated, the unstable complex conjugate poles correspond to frequencies $mf_0 \pm f_s$ ($m \in \mathbb{N}$). Nevertheless, for the finite frequency band under analysis, only poles with frequencies f_s and $f_0 \pm f_s$ will appear.
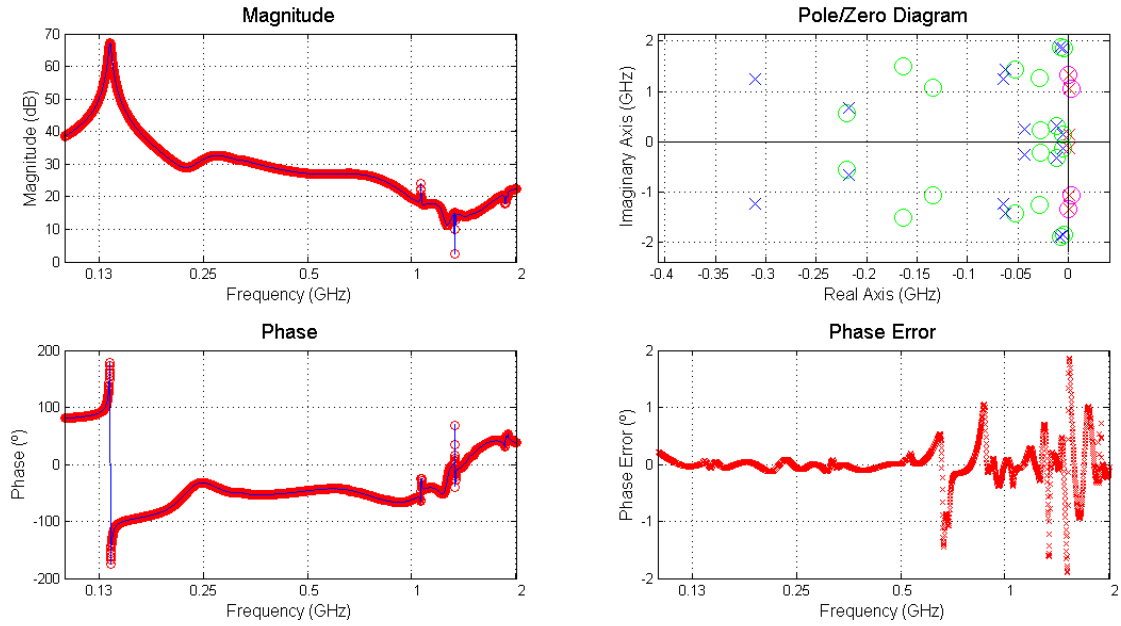
Figure 4.22: Identification results of the frequency response simulated in the second stage of the L-band amplifier with input power $P_{in} = -6\,\mathrm{dBm}$, carried out by our algorithm and *after* the last cleaning.

From Figure 4.22 we observe that after the last cleaning of spurious poles the maximum phase error raises up to 2°. Therefore, as stated in the Section 4.1, this value can be taken as a more suitable phase tolerance for the identification in hand. Indeed, if we perform once again the identification of Figures 4.21 and 4.22 with our algorithm and $\theta_{tolerance} = 2°$, we obtain te following results:

Figure 4.23: Result of the identification of the simulated frequency response with input power $P_{in} = -6\,\mathrm{dBm}$, *before* the last cleaning of spurious poles and with $\theta_{tolerance} = 2°$.

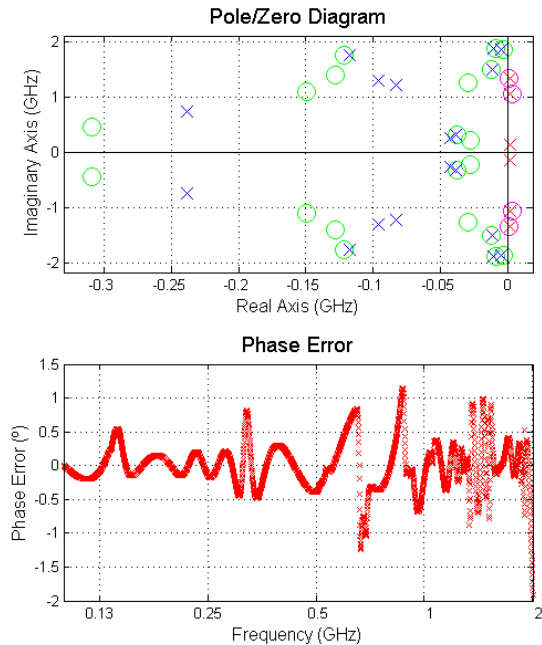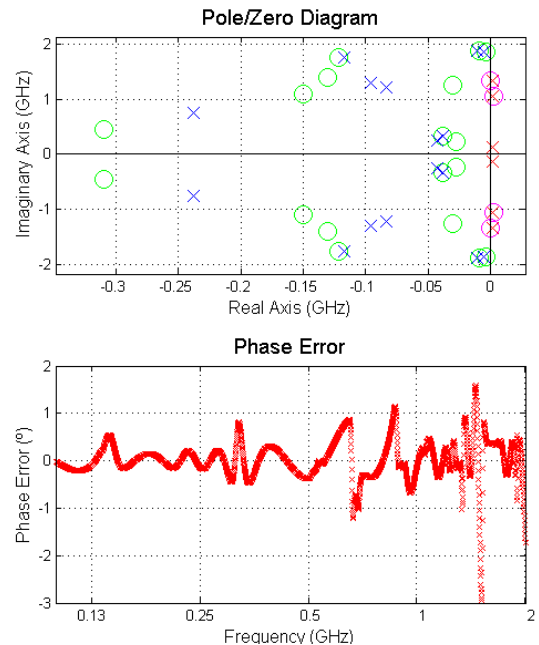Figure 4.24: Result of the identification of the simulated frequency response with input power $P_{in} = -6\,\mathrm{dBm}$, *after* the last cleaning of spurious poles and with $\theta_{tolerance} = 2°$.

From the previous Figures 4.23 and 4.24, we can state that $\theta_{tolerance} = 2^{\circ}$ is a more suitable phase tolerance for this type of frequency responses, since all the unstable poles are clearly detected and the number of quasi-canceled poles on the left-hand-side of the plane is considerably decreased (compared to Figures 4.22 and 4.21, obtained with default $\theta_{tolerance} = 0.5^{\circ}$).

These identifications have been performed with simulated frequency responses, that is, they have only been influenced by the numerical noise of the simulation. Hence, both *MM_stab* and our tool have shown similar outcomes. Nevertheless, the identification of measured frequency responses is more critical and indeed, noise from experimental measures causes the differences between the two algorithms to emerge.

For this reason, we will finish the section by analyzing a number of frequency responses (of this same amplifier) that have been obtained by an experimental technique based on the use of a high-impedance probe and proposed in [21]. They have been measured with no input power and accordingly, correspond to the DC steady state. For no input power, no oscillations are encountered. However, it has been observed that with fixed $V_{GG} = -2.1\,\mathrm{V}$, the pair of complex conjugate poles at frequency f_s approaches the imaginary axis as V_{DD} is increased [21]. Therefore, the stability margin is decreased and they become critical poles. Their evolution is represented in Figure 4.25, obtained varying V_{DD} from $1\,\mathrm{V}$ to $15\,\mathrm{V}$.
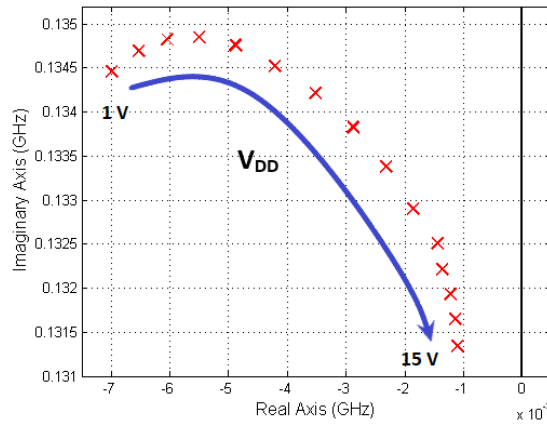

Figure 4.25: Evolution of the critical pair of poles *vs.* V_{DD}, varied from $1\,\mathrm{V}$ to $15\,\mathrm{V}$. For sake of clarity, only the positive frequencies (positive imaginary part) have been plotted.

Obviously, considering that these responses are obtained from a measured DC stable steady state, only stable poles ought to be identified. In order to gather a significant sample of responses, we will vary V_{DD} from 1 V to 15 V, in steps of 1 V. Likewise, to complete the examination of the validity of our algorithm, we will perform the same identifications with the state-of-the-art automatic algorithm[6].

For high values of V_{DD} —when the pole is closer to the imaginary axis— and default phase tolerance $\theta_{tolerance} = 0.5^{\circ}$, *both* algorithms identify unstable poles or zeros, as it is a more critical situation. In fact, in order to only obtain stable poles, the phase $\theta_{tolerance}$ must be increased[7] up to 2°. Nevertheless, for lower values of V_{DD} our algorithm excels. For instance, for $V_{DD} = 2\,\mathrm{V}$, *MM_stab* identifies one couple of quasi-canceled unstable pole-zeros, whereas our algorithm only identifies stable poles after the last cleaning. This is shown in Figures 4.26, 4.27 and 4.28, where the results of the identifications carried out by *MM_stab* and by our tool (before and after the last cleaning) are depicted, respectively.

---

[6]All the identifications will be carried out in the second stage and with default setting for both algorithms, specially $\theta_{tolerance} = 0.5^{\circ}$.
[7]It must be considered that measured frequency responses contain noise and that $\theta_{tolerance} = 0.5^{\circ}$ might not be the most adequate value for all of them.

Figure 4.26: Result of the identification of the measured frequency response corresponding to the DC steady state with $V_{DD} = 2\,\text{V}$, carried out by *MM_stab*.

Figure 4.27: Result of the identification of the measured frequency response corresponding to the DC steady state with $V_{DD} = 2\,\text{V}$, carried out by our tool and *before* the last cleaning.
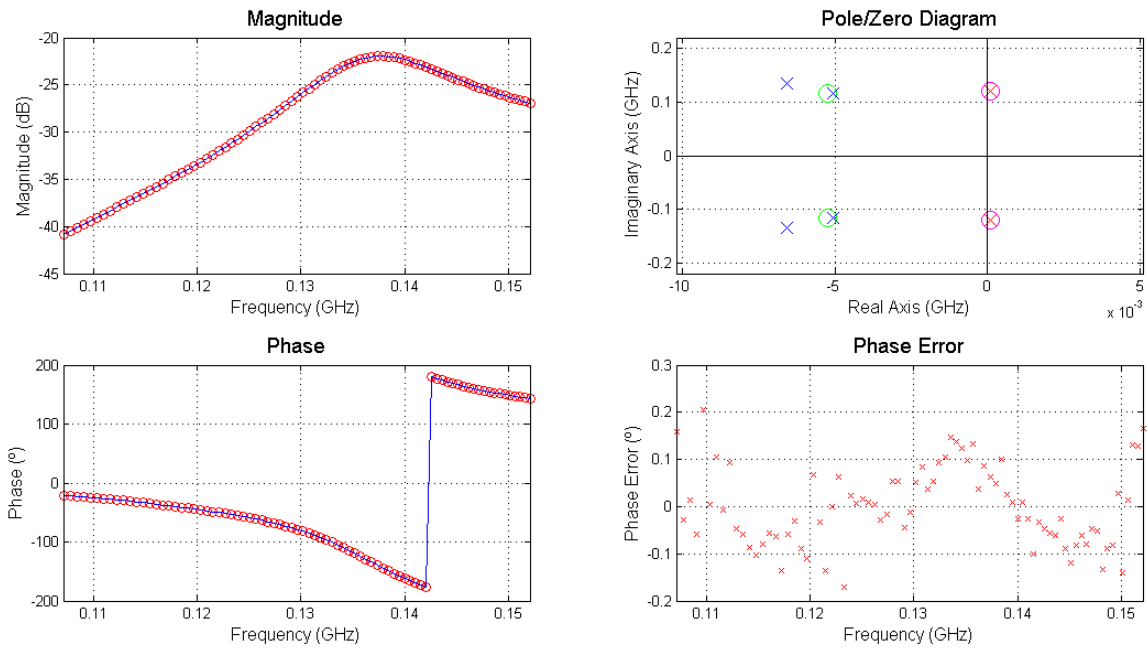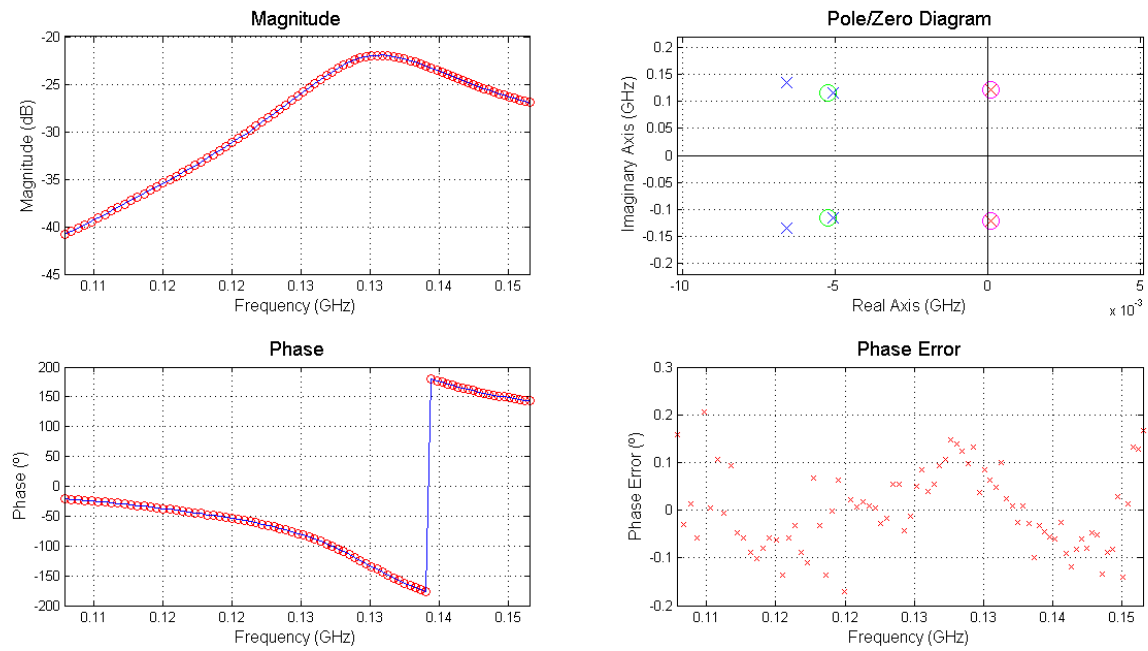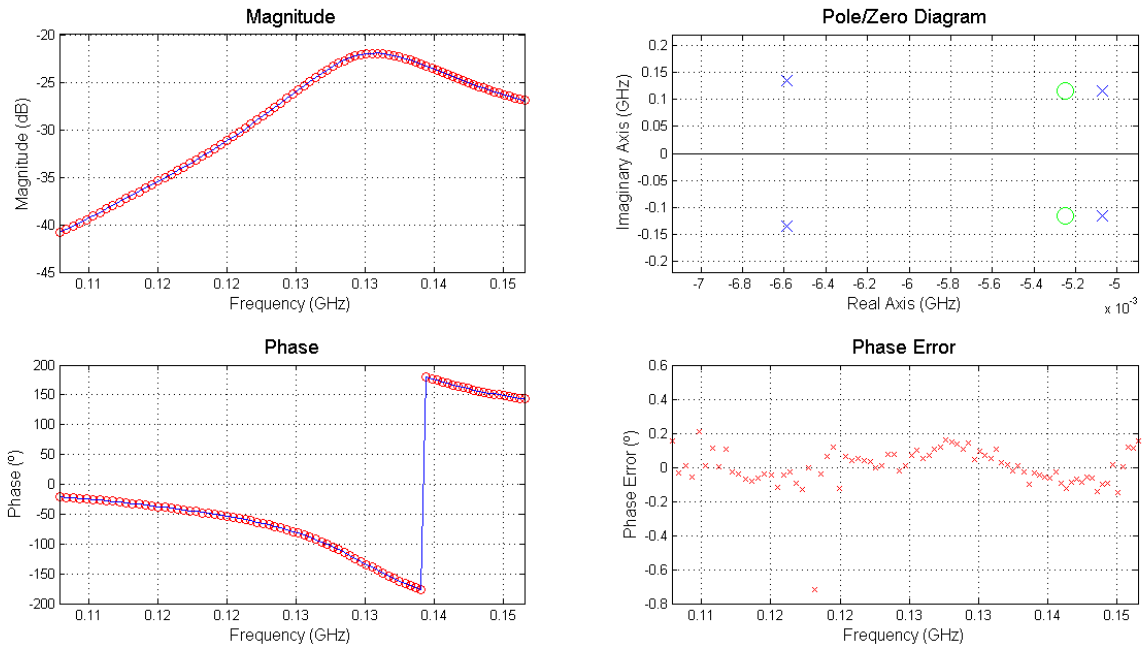
Figure 4.28: Result of the identification of the measured frequency response corresponding to the DC steady state with $V_{DD} = 2\,\mathrm{V}$, carried out by our tool and *after* the last cleaning.

From Figure 4.27, we observe that our algorithm has identified an unstable numerical quasi-cancellation. Still, after the last cleaning of spurious poles (as seen in Figure 4.28), this false instability is suppressed and only two pairs of stable complex conjugate poles remain. In addition, we can notice that the phase error is increased up to 0.7º; that is, the fitting goal is no longer respected. However, as detailed in Section 4.1, this can serve as an estimated value of a more suitable phase tolerance for the identification of this type of frequency responses. Indeed, performing these same identifications with $\theta_{tolerance} = 0.7$º for low V_{DD} values, we have evidenced significant improvements with both algorithms.

To conclude, we can state that this study has proved the validity and reliability of our algorithm regarding the stability analysis of a real RF amplifier. For simulated responses, no substantial differences have been found between the two automatic algorithms. However, for measured responses, our algorithm has proved to provide better results in certain cases. Furthermore, it has provided an estimation of a more adequate phase tolerance for this certain type of frequency responses.

Chapter 5

Conclusions

In this last chapter, we will conclude the report by recapitulating the improvements introduced by our algorithm to the state-of-the-art automatic VF identification for stability analysis. Likewise, we will outline its limitations and propose different ideas for further work.

The main innovation of this project has been the introduction of three novel steps conceived for the convergence improvement —in the event of noise— to the context of over-modeling of pole-zero identification: a meticulous placing of the added poles, a threshold relative error between successive iterations and a cleaning of spurious poles.

As evidenced in the analytical comparison carried out in Chapter 4, these contributions to the state-of-the-art algorithm have resulted in an overall decrease of the order of identification. In the first place, we have proved that the meticulous placing of the added poles and the extra stopping condition of the identification loop can help to reduce the order of the transfer function. Moreover, the last cleaning of spurious poles has proved to be very powerful in the detection and elimination of numerical pole-zero quasi-cancellations, as we have clearly seen in Section 4.1.

Furthermore, the display of the results both *before* and *after* the last cleaning of spurious poles provides useful information regarding the identification and its limitations. For instance, as previously explained, the maximum value of the phase error after the last cleaning can serve as an estimation of a more suitable phase tolerance for that type of frequency responses.

Therefore, our algorithm implemented in *Matlab* has resulted in a pole-zero identification stability analysis tool as reliable and efficient as the commercial ones and, in addition, generally less sensitive to over-modeling. It must be emphasized that although we have not precisely analyzed MIMO responses, our method is also able to perform pole-zero identifications to these kind of responses. Most importantly, we have verified that it is equally reliable for the identification and stability analysis of real RF and microwave amplifiers. In fact, the method proposed in [11] was only tested with analytical frequency responses, created *ad hoc*, and with our tool we have corroborated the validity of this technique for more realistic frequency responses.

Nevertheless, even though it has proved to reduce over-modeling, some limitations have been detected related to noise and physical quasi-cancellations. As proved in Section 4.1, in the event of a very strong physical quasi-cancellation in a highly noisy response, our algorithm suppresses the physical quasi-cancellation after the last cleaning of spurious poles. As a consequence, together with the analysis of the d_n factor formerly explained, a MIMO or parametric analysis is suggested in that event, in order to distinguish a true physical quasi-cancellation from a numerical one. However, it must be emphasized that the quasi-cancellation being so strong and the noise so high, the quasi-canceled pole-zero are "hidden" inside the noise and therefore, this identification problem is not a limitation of our algorithm *per se*.

In addition, due to its more complex structure, the identification carried out by our algorithm can sometimes be slower and more troublesome regarding convergence. In such cases, it is only necessary to relax the error variation threshold α, the spurious poles discriminator γ and the minimum distance delimiter ν.

However, to sum up, we can state that it is a rather promising work and that it has accomplished the objectives proposed in the Section 1.2. In addition, further work could involve the study of the weighting in the identification and a deeper examination regarding the influence of the proposed parameters. In fact, for each type of noise some kind of weighting function and parameters can be more suitable than others. The algorithm could also be formalized and implemented for MIMO and parametric analysis.

Bibliography

[1] A. Suárez and R. Quere, *Stability Analysis of Nonlinear Microwave Circuits.* Norwood, MA, USA: Artech House, Inc., 2 ed., 2003.

[2] A. Suárez, *Analysis and Design of Autonomous Microwave Circuits.* Hoboken, NJ, USA: John Wiley & Sons, 1 ed., 2009.

[3] V. Rizzoli and A. Neri, "State of the Art and Present Trends in Nonlinear Microwave CAD Techniques," *IEEE Trans. Microw. Theory Tech.*, vol. 36, no. 2, pp. 343-365, 1988.

[4] J.M. Rollett, "Stability and Power-Gain Invariants of Linear Twoports," *IRE Trans. Circuit Theory,* vol. 9, no. 1, pp. 29-32, 1962.

[5] M. Ohtomo, "Proviso on the Unconditional Stability Criteria for Linear Twoport," *IEEE Trans. Microw. Theory Tech.*, vol. 43, no. 5, pp. 1197-1200, 1995.

[6] A. Platzker, W. Struble and K. T. Hetzler, "Instabilities Diagnosis and the Role of K in Microwave Circuits," *in IEEE MTT-S Int. Microw. Symp. Dig.*, (Atlanta, GA, USA), pp. 1185-1188, IEEE, June 1993.

[7] C. Barquinero, A. Suárez, A. Herrera and J.L. García, "Complete Stability Analysis of Multifunction MMIC Circuits," *IEEE Trans. Microw. Theory Tech.*, vol. 55, no. 10, pp. 2024-2033, 2007.

[8] J. Jugo, J. Portilla, A. Anakabe, A. Suarez and J.M. Collantes, "Closed-loop stability analysis of microwave amplifiers," *Electronics Letters*, vol. 37, no. 4, pp. 226-228, 15 Feb 2001.

[9] R. Pintelon and J. Schoukens, *System Identification: A Frequency Domain Approach.* New York, NY, USA: Wiley-IEEE Press, 2 ed., 2012.

[10] L. Mori, "Stability analysis of RF power amplifiers through MIMO pole-zero identification techniques," Ph.D. dissertation, University of the Basque Country (UPV-EHU), 2019.

[11] S. Grivet-Talocia and M. Bandinu, "Improving the convergence of vector fitting for equivalent circuit extraction from noisy frequency responses," *IEEE Transactions on Electromagnetic Compatibility*, vol. 48, no. 1, pp. 104-120, Feb. 2006.

[12] S. Skogestad and I. Postlethwaite, *Multivariable Feedback Control: Analysis and Design.* New York, NY, USA: John Wiley & Sons, 1996.

[13] J.M. Collantes, L. Mori, A. Anakabe, N. Otegi, I. Lizarraga, N. Ayllón, F. Ramírez, V. Armengaud and G. Soubercaze-Pun, "Stability Analysis with Pole-Zero Identification: Unveiling the Critical Dynamics of Microwave Circuits," *IEEE Microwave Magazine*, vol. 20, no. 7, pp. 36-54, Jul. 2019.

[14] N. Ayllon, J.M. Collantes, A. Anakabe, I. Lizarraga, G. Soubercaze-Pun and S. Forestier, "Systematic Approach to the Stabilization of Multitransistor Circuits," *IEEE Transactions on Microwave Theory and Techniques*, vol. 59, no. 8, pp. 2073-2082, Aug. 2011.

[15] A. Anakabe, N. Ayllon, J.M. Collantes, A. Mallet, G. Soubercaze-Pun and K. Narendra, "Automatic pole-zero identification for multivariable large-signal stability analysis of RF and microwave circuits," in *40th Eur. Microw. Conf.*, (Paris, France), pp. 477-480, Sep. 2010.

[16] A. Semlyen and B. Gustavsen, "Rational Approximation of Frequency Domain Responses by Vector Fitting," *IEEE Trans. Power Deliv.*, vol. 14, no. 3, pp. 1052-1061, 1999.

[17] A. Semlyen and B. Gustavsen, "Vector Fitting by Pole Relocation for the State Equation Approximation of Nonrational Transfer Matrices," *Circuits, Syst. Signal Process.*, vol. 19, no. 6, pp. 549-566, 2000.

[18] B. Gustavsen, "Improving the Pole Relocating Properties of Vector Fitting," *IEEE Trans. Power Deliv.*, vol. 21, no. 3, pp. 1587-1592, 2006.

[19] L. Mori, "Stability Analysis of RF amplifiers based on MIMO pole-zero identification," Bachelor Final Project, University of the Basque Country (UPV-EHU), 2014.

[20] L. Mori, A. Anakabe, I. Lizarraga, N. Otegi, J.M. Collantes, V. Armengaud and G. Soubercaze-Pun, "Stability analysis of multistage power amplifiers using Multiple-Input Multiple-Output identification," in *IEEE MTT-S Int. Microw. Symp. Dig.*, (San Francisco, CA, USA), pp. 1-4, May 2016.

[21] J.M. Gonzalez, N. Otegi, A. Anakabe, L. Mori, A. Barcenilla and J.M. Collantes, "In-Circuit Characterization of Low-Frequency Stability Margins in Power Amplifiers," *IEEE Transactions on Microwave Theory and Techniques*, vol. 67, no. 2, February 2019.